Computed Tomography and Magnetic Resonance Imaging in Determination of Human Body Composition

Methodological and Applied Studies

John Brandberg MD

UNIVERSITY OF GOTHENBURG

Department of Radiology
Institute of Clinical Sciences

Sahlgrenska Academy
University of Gothenburg
Sweden
2009

John Brandberg

Department of Radiology
Institute of Clinical Sciences

Sahlgrenska Academy
University of Gothenburg
Sahlgrenska University Hospital
SE-413 45 GOTHENBURG
Sweden

ISBN 978-91-628-7698-2
http://hdl.handle.net/2077/19048
Printed in Gothenburg, Sweden, by Intellecta DocuSys

To my family Christina, Carl, Erik, and Oskar

Abstract

Background: Computed tomography (CT) and magnetic resonance imaging (MRI) provide important research opportunities due to their unique capability of characterizing and quantifying tissues and organs. Ionizing radiation is a limitation using CT, and recent developments aiming to improve MRI for determination of body composition have not been validated. An area with special interest in body composition is obesity research. The prevalence of obesity is increasing and abdominal, in particular visceral, obesity is associated with the metabolic syndrome and type 2 diabetes.

Aims: I. To evaluate if the radiation dose to the subject can be substantially reduced in assessment of body composition using CT while maintaining accurate measurements of adipose and muscle tissue areas and muscle tissue attenuation. II. To validate a T1 mapping whole-body MRI method, used for assessment of body composition, by comparing it with a whole-body CT method. III. To examine within-scanner reproducibility and between-scanner performance of CT measurements of adipose and muscle tissue areas and liver attenuation. IV. To study the effects of GH treatment on body composition and insulin sensitivity in postmenopausal women with abdominal obesity.

Methods: I. Seventeen subjects, covering a wide range of body diameters, were examined using scan parameters chosen to reduce radiation dose as well as standard clinical scan parameters. Tissue areas and muscle CT-numbers were measured. II. Ten patients were examined both by MRI and CT to validate the T1 mapping whole-body MRI method. MRI and CT results were compared regarding tissue areas and volumes, slice by slice, and for the whole body, respectively. III. Reproducibility of the two CT scanners was investigated using duplicates from 50 patients. Between-scanner performance was evaluated by comparison of results from 40 patients. IV. The effects of GH treatment were studied in 40 women in a randomized, placebo-controlled 12-month trial. Changes in body composition and insulin sensitivity were evaluated using CT and clamp-technique, respectively.

Results and conclusions: I. In assessment of body composition using CT, the radiation dose to the subject was reduced to 2-60 % of standard dose used for diagnostic purposes while maintaining accurate measurements of adipose and muscle tissue areas and muscle tissue attenuation,. The resulting effective dose for a single slice examination is <0.1mSv, a dose level associated with trivial risk. Therefore, CT can be justified for body composition assessment even in large populations or for repeated examinations. II. Compared with CT, the MRI method slightly overestimated subcutaneous adipose tissue volume and slightly underestimated visceral adipose tissue volume, but it can be considered sufficiently accurate for whole-body measurements of adipose tissue volumes. III. Within-scanner reproducibility and between-scanner agreement were high for measurements of adipose and muscle tissue area. For measurements of liver attenuation, within-scanner reproducibility was high while a systematic bias was revealed in comparison between scanners. Therefore, comparison of CT numbers for liver from different scanners may be unreliable. IV. GH treatment of postmenopausal women with abdominal obesity reduced visceral adipose tissue and improved insulin sensitivity. CT revealed adipose tissue changes not detectable by waist-to-hip ratio, sagittal diameter, or waist circumference.

Keywords: X-ray Computed Tomography, Magnetic Resonance Imaging, Body Composition, Obesity, Metabolic Syndrome X, Glucose Metabolism, Growth Hormone, Fatty Liver, Intra-Abdominal Fat.

ISBN 978-91-628-7698-2 Gothenburg 2009
http://hdl.handle.net/2077/19048

This thesis is based on the following original papers

I Brandberg J, Lönn L, Bergelin E, Sjöström L, Forssell-Aronsson E, Starck G.
Accurate tissue area measurements with considerably reduced radiation dose achieved by patient-specific CT scan parameters
Br J Radiol. 2008; 81 (October), 801-808.

II Kullberg J, Brandberg J, Angelhed J-E, Frimmel H, Bergelin E, Strid L, Ahlström H, Johansson L, Lönn L.
Whole-body adipose tissue analysis: comparison of MRI, CT and dual energy X-ray absorptiometry
Br J Radiol. 2009; 82 (February), 123-130.

III Brandberg J, Lönn L, Lantz H, Torgerson JS, Angelhed J-E, Lönn M, Sjöström L.
Computed tomography determination of body composition in multi-center studies. A comparison of two CT-systems
Manuscript.

IV Franco C, Brandberg J, Lönn L, Andersson B, Bengtsson BÅ, Johannsson G.
Growth hormone treatment reduces abdominal visceral fat in postmenopausal women with abdominal obesity: a 12-month placebo controlled study
J Clin Endocrinol Metab. 2005; 90 (March), 1466-1474.

Contents

Abbreviations

AT	Adipose tissue
BF	Body fat
BM	Bone marrow
BMD	Bone mineral density
BMI	Body mass index
BW	Body weight
CI	Confidence interval
CT	Computed tomography
CV	Coefficient of variation
DXA	Dual energy x-ray absorptiometry
FFM	Fat free mass
FOV	Field of view
GDR	Glucose disposal rate
GH	Growth hormone
HDL	High-density lipoprotein
HOMA-IR	Homeostasis model assessment of the insulin resistance index
HPLC	High-pressure liquid chromatography
HU	Hounsfield unit
IDF	International Diabetes Federation
IGF-I	Insulin-like growth factor I
IGT	Impaired glucose tolerance
IMAT	Inter-muscular adipose tissue
LDL	Low-density lipoprotein
LT	Lean tissue
LTM	Lean tissue mass
MRI	Magnetic resonance imaging
MT	Muscle tissue
NAFLD	Non-alcoholic fatty liver disease
NASH	Non-alcoholic steatohepatitis
NCEP ATP III	National Cholesterol Education Program, Adult Treatment Panel III
NMR	Nuclear magnetic resonance
OGTT	Oral glucose tolerance test
OLR	Ordinary linear regression analysis
RIA	Radio-immuno-assay
ROI	Region of interest
SAT	Subcutaneous adipose tissue
SD	Standard deviation
SE	Standard error
SEM	Standard error of the mean
SIB-pair	Sibling pair
SOS	Swedish obese subjects study
T2D	Type 2 Diabetes mellitus
TG	Triglyceride
VAT	Visceral adipose tissue
WC	Waist circumference
WHO	World Health Organisation
WHR	Waist hip ratio
XENDOS	XENical® in the prevention of Diabetes in Obese Subject

Introduction

Medical imaging

In November 1895, the German physicist Wilhelm C. Röntgen accidently discovered x-rays also called Röntgen rays after its discoverer. Only a few months later skeletal fractures were imaged and medical imaging had commenced. For his discovery, Röntgen was awarded the first Nobel Prize in Physics in 1901. The technique spread quickly all over the world and in May 1896 an x-ray tube that had been constructed for teaching purposes was used by the Gothenburg surgeon Alrik Lindh to localize shotgun shots in an arm of a patient (1).

Computed tomography (CT) was invented by Allan M Cormack and Sir Godfrey N Hounsfield. Cormack performed the theoretical calculations for the technique in 1963. Unfortunately, there was not enough computing power available at the time for a practical implementation. Hounsfield, independently of Cormack conceived the idea of CT during a weekend ramble in 1967. Initially it had nothing to do with medicine but was simply "a realisation that you could determine what was in a box by taking readings [of x-rays] at all angles through it" (2). Hounsfield built the first CT scanner and the first human patient was scanned in October 1971. A new era in medical imaging had started. The technique was quickly spread all over the world. The first scanner in Sweden was installed at Karolinska Institutet in 1973 (3). Cormack and Hounsfield were awarded the Nobel Prize in Physiology or Medicine in 1979.

Nuclear magnetic resonance (NMR) in matter of “ordinary density” was first demonstrated in 1946 by Edward Purcell and Felix Bloch. They were awarded the Nobel Prize for their discovery in 1952. NMR spectroscopy became a fundamental technique in analytical chemistry used in the study of molecules. It was not until the 1970’s that the development of magnetic resonance imaging (MRI) started when Paul Lauterbur and Sir Peter Mansfield devised and developed the principles for imaging based on NMR. Frequency encoding during signal readout by a magnetic field gradient, devised by Lauterbur and selective radio frequency irradiation to excite a single slice, introduced by Mansfield are key elements for spatial encoding of the signal in MRI. In 1976 Mansfield and co-workers managed to produce a cross sectional image of a finger. Lauterbur and Mansfield were awarded the Nobel Prize in Physiology or Medicine in 2003. Raymond Damadian built the first “full-body” MRI machine and produced its first magnetic resonance image of the human body in 1977. Even though many years have past since CT and MRI were introduced, refined methods for investigation of the human body using these techniques are still being developed. Detailed imaging of pathological morphology and function as well as anatomical and physiological properties leads to new insights in medical research and new possibilities for early detection and evaluation of disease. Different tissues in the body e.g. adipose tissue and muscle tissue are easily distinguished in both CT and MRI images. Both techniques have therefore been used for body composition applications on a tissue level.

Obesity

According to the World Health Organisation (WHO) overweight and obesity are defined as abnormal or excessive fat accumulation that presents a risk to health. A crude population measure of obesity is the body mass index (BMI), *i.e.* a person’s weight (in kilograms) divided by the square of his or her height (in metres). A person with a BMI of 30 kg/m^2 or more is generally considered obese. A person with a BMI ≥ 25 kg/m^2 is considered overweight, table 1. Persons with a BMI ≥40 kg/m^2 are defined as extremely obese (4). In studies, evaluating surgery as treatment of obesity further levels have been described, *e.g.* ≥50, super obese; ≥60; super-super obese; ≥70, extremely super obese. These levels of obesity are, however, not officially recognized as weight categories (5). The increasing prevalence of obesity constitutes a major health problem (6).

Table 1. Weight categories based on BMI

BMI	Definition
Below 18.5	Underweight
18.5 to 24.9	Healthy weight
25.0 to 29.9	Overweight
30 or higher	Obesity

In the United States, 32 % of adults were obese in 2003-2004 and from 1999 to 2004 the prevalence increased among children, adolescents and adult males (7). In Sweden the prevalence is lower and is now approximately 10 % in both men and women (8). Overweight and obesity are major risk factors for a number of chronic diseases, including cardiovascular diseases, cancer, and type 2 diabetes (T2D). Therefore, obesity is associated with an increased morbidity and mortality (9-11). Of patients with T2D 80-90 % are overweight or obese (12). Obesity is strongly associated with impaired glucose tolerance and insulin resistance (6, 12). There are several adipose tissue depots and differences in distribution between individuals. The male type of obesity is characterized by increased adipose tissue in the abdominal region and the female type of obesity is characterized by increased adipose tissue of the thighs, buttocks, and legs. More specifically, the male type of obesity is associated with an increased amount of visceral adipose tissue (VAT) depots while the female type of obesity is associated with an increased amount of subcutaneous adipose tissue (SAT) (13). Figure 1 shows the distribution of adipose tissue, as determined by CT, in a male and a female subject, both with a BMI of 33 kg/m^2. Increased fat accumulation in VAT, intermuscular adipose tissue (IMAT), as well as in liver, and muscle cell has been shown to be associated with insulin resistance (14-17).

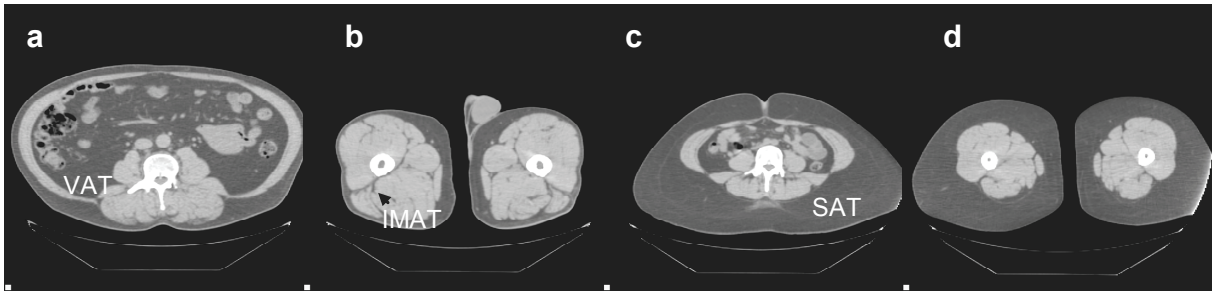

Figure 1. Cross section of the abdomen (a, c) and thighs (b, d) by computed tomography. A male (a, b) and a female (c, d) subjects, both with a BMI of 33 kg/m^2. In the male subject there is an increase in visceral tissue (VAT) and in the female subject there is an increase in the subcutaneous adipose tissue (SAT). The intermuscular adipose tissue (IMAT, arrow) is also illustrated.

The metabolic syndrome

In 1988 the current concept of the metabolic syndrome was introduced by Reaven, who described the cluster of insulin resistance, hyperinsulinaemia, glucose intolerance, hypertension, raised triglyceride concentration, and low high density lipoprotein cholesterol concentration (18). Together these form an essential part of the clinical features of the metabolic syndrome (19-21). The first most widely spread definition of the metabolic syndrome was the one coming from the WHO in 1999 (20). In the following years the scientific focus on central obesity increased and the definition from National Cholesterol Education Programme Adult Treatment Panel III (NCEP ATP-III) in 2001 (21) reflects this, using waist circumference as a measure of central obesity instead of waist-hip ratio which is the criteria used by the WHO. The updated version of NCEP ATPIII from 2004 (22) and the International Diabetes Federation's (IDF) definition from 2005 (23) are similar. A meeting in 2006 tried to reach consensus to recommend the IDF definition, but the definition of the syndrome is still debated (19). There is a summary of the definitions in table 2. The definitions of the metabolic syndrome can include patients with T2D. For patients with the metabolic syndrome but without T2D there is a drastically increased risk of developing T2D.

Table 2. Definitions of the metabolic syndrome

		WHO	NCEP ATP III	IDF
		1999	2001 (modified 2004)	2005
		Glucose intolerance, IGT or diabetes and/or insulin resistance with two or more of the following risk factors	Three or more of the following risk factors	Three or more of the following risk factors
Fasting plasma-glucose (mmol/L)			≥5.6	≥5.6
Arterial blood pressure (mmHg)		>140/90	≥130/85	≥130/85
Serum-HDL-Cholesterol (mmol/L)	men		<1.29	<1.29
	women		<1.03	<1.03
Serum-triglyceride level (mmol/L)		≥1.7 mmol/l	≥1.7 mmol/l	≥1.7 mmol/l
Obesity	men	WHR>0.90	WC >102	WC >94
	women	WHR>0.85	WC >88	WC >80
Microalbuminuria		Urinary albumin excretion rate ≥20µg/min or albumin/creatinine ratio ≥30µg/g		

WHO, World Health Organization
NCEP ATP III, The National Cholesterol Education Program Adult Treatment Panel III
IDF, International Diabetes Federation
IGT, impaired glucose tolerance
HDL, high-density lipoprotein
WHR, waist hip ratio
WC, waist circumference

Fatty liver disease

With the increasing prevalence of obesity, the metabolic syndrome and T2D in the general population (12), non-alcoholic fatty liver disease (NAFLD) has become the most common cause of chronic liver disease in the United States (24). The prevalence of NAFLD is up to 31 % in the population, 50 % in people with diabetes and 74 % in obese individuals (24, 25). It has been suggested that NAFLD should be a feature of the metabolic syndrome (16). NAFLD is usually limited to steatosis but it can develop into the more serious condition of non-alcoholic steatohepatitis (NASH) (26). NASH is characterized by liver steatosis and inflammation with or without fibrosis (27). Significant weight gain and insulin resistance is associated with progression of liver fibrosis (28). NASH can lead to end-stage liver disease, *i.e.* cirrhosis which may require transplantation (29).

Growth Hormone and body composition

Growth hormone (GH) is a peptide hormone synthesized and secreted in a pulsatile manner from the somatotrope cells of the anterior pituitary gland. GH secretion decreases with increasing age and obesity. Physical activity increases GH secretion and thus physical fitness is associated with higher GH levels. GH stimulates production of insulin-like growth factor I (IGF-I) in peripheral tissues, but the main source of circulating IGF-I is the liver. GH has direct effects on target tissues but some effects are indirect by autocrine, paracrine and endocrine actions of IGF-I, mediated by hepatic IGF-I. GH is normally considered to have anti-insulin actions, whereas insulin-like growth factor I (IGF-I) has insulin-like actions.

In healthy, non-obese men and women, the amount of visceral adipose tissue has a strong negative exponential relationship with mean 24-hour serum GH concentrations (30). Further, GH deficient adults are disposed to insulin resistance and share many of the features of the metabolic syndrome (31, 32). Several studies in GH deficient adults have shown that GH replacement improves the body composition profile (33, 34). A study with a crossover six-month open treatment trial of GH deficient adults showed a 16 % reduction of total adipose tissue (AT) measured by CT. The largest relative decrease, 32 %, was seen in the VAT depot (35). In the same study, the total muscle tissue (MT) volume increased 5.1 % with the relatively largest increase in the arms and legs, 14.3 % and 7.6 %, respectively. The opposite changes were seen in a one-year trial of surgically treated patients with acromegaly (36). The total AT depot in women increased 20 % and the MT depot decreased 12 % during the treatment. In the same study, the overall changes in men were more prominent than in women. This improvement in distribution of AT is not always linked to improvements in insulin sensitivity presumably due to the anti-insulin effects of GH therapy. GH treatment has major effects on lipolysis, which may be one of the mechanism to promote its anti-insulin effects.

Assessment of body composition

The term body composition implies that the body can be divided into compartments. This division can be made in many ways but common for all divisions is that the sum is the human body, usually defined by body weight. Wang and co-workers constructed a model of different levels used for these divisions (37). The five levels are atomic, molecular, cellular, tissue system and whole body. In our studies, assessment of body composition was performed on several of these levels, *e.g.* counting of the radioactivity from the potassium isotope ^{40}K in a whole-body γ counter on the atomic level; determination of body fat by DXA on the molecular level; measurements of adipose tissue by CT and MRI on the tissue system level, and, anthropometry on the whole-body level. Body composition varies between individuals. These variations can be linked to differences in among other things gender, age, race, and genome. Changes in food intake and physical activity as well as actions of several hormones *e.g.* growth hormone can also influence body composition.

Anthropometry

Anthropometry [Greek] literally means "measurements of humans". A common measure of obesity apart from weight is BMI. Increased BMI is used as a criterion of obesity in almost all studies even though it does not take into account the amount of the different tissues such as muscle tissue and adipose tissue that contribute to the body weight. Therefore, this surrogate measure of obesity can give misleading results (38, 39). Waist circumference (WC) is an estimate of central obesity according to the NCEP ATPIII and the IDF definitions of the metabolic syndrome, table 2 (19, 21, 40). Waist-to-hip ratio (WHR) is also used as a measure of central adiposity and is calculated as the waist circumference divided with the hip circumference (20, 40). The sagittal abdominal diameter has been shown to be a marker of especially visceral adiposity (40). Anthropometrical methods are readily available, cheap and, easy to perform although training is required to reach a high level of reproducibility (41).

Total body potassium

Total body potassium is a measurement on the atomic level of Wang's model. There are three naturally distributed isotopic states of potassium. The gamma-emitting isotope ^{40}K constitutes 0.0118 % of the total potassium in the body. Potassium is located mainly in the fat free mass (FFM) and the potassium content in FFM is estimated at an average 62 mmol/ kg in women (42, 43). When the FFM has been determined the body fat (BF) can be calculated as the body weight (BW) subtracted by the FFM. The method requires a whole body γ counter that is available only at a limited number of research centres. There are several challenges in the calibration of the instrument and it is sensitive to background interferences demonstrated by the transient increase in caesium radioisotopes released in the Chernobyl accident (44).

Dual energy X-ray absorptiometry

When an object is exposed to x-rays, only a part of the photons will penetrate. The properties of the object determine the fraction of photons that will reach the detector and this is related to the attenuation of the x-ray beam by the object. Dual energy x-ray absorptiometry (DXA) measures the attenuation of x-rays from two sources with different levels of photon energies. The penetration of photons is higher with higher energy levels and thus the detector receives two different measurements for each pixel (picture element). In projections where no bone is present, the soft tissue is composed of fat and lean. Thus in each pixel of soft tissue the ratio of the values at high energy level and low energy level R_{st} is proportional to the proportions of fat and lean. By comparing the ratio for soft tissue R_{st} with measures of the ratio for pure fat, R_f , lean R_l can be calculated by solving the equation below, equation 1. In this way, the proportions of lean and fat are determined in each pixel. The attenuation for fat used for the calculation is from pure fat *i.e*. triglycerides, making DXA a measurement on the molecular level. In areas containing bone, the proportions of fat and lean is estimated from adjacent soft tissue areas. Determination of bone mineral content and bone mineral density is the most common use of DXA. Bone mineral density (BMD) derived from DXA is actually BMD area (g/cm^2). The DXA equipment manufacturers do not reveal the details of these assumptions. Thus from DXA the following can be derived; the body mass constitutes of fat mass and fat-free mass. The latter can be divided into total body bone mineral and bone free lean tissue mass. DXA equipment is widely spread and mainly used for bone density measurements. However, the same equipment can be used for body composition studies. The examination imparts a low radiation dose to the subject and is easy to perform and analyse.

(Equation 1)

$$R_{st} = \frac{R_{st} - R_f}{R_l - R_f}$$

Computed tomography

To produce a computed tomography (CT) image the x-ray source and the detector are rotated in an arc (usually 360°) around a cross section of the object. During the rotation multiple measurements of photons reaching the detectors are made, resulting in a set of projections through the tomographic section. The fraction of photons reaching the detector is a measure of the attenuation of the x-ray beam through the tomographic section in the object. After recalculation of the detector data a set of attenuation profiles is obtained and used to reconstruct an image of the tomographic section. During calibration the scanner is set to measure air as −1000 Hounsfield units (HU) (representing principally no attenuation) and water as 0 HU. This scale of CT numbers is then transformed to a gray-scale image with pixels which represent the attenuating properties of each voxel (volume element) measured. If the volume contains a homogeneous tissue the pixel will have the CT number typical for this tissue. Volumes which contain a mixture of tissues with diverse attenuating properties, will have an averaged CT number, which is related to the proportions of the tissues. This effect is called partial volume artefact. The effect is dependent of the voxel size corresponding to the reconstructed pixels (45). An examination by CT for determination of body composition is a rapid procedure, that is easy to perform and the equipment is widely spread. However, the radiation dose can limit its usefulness especially in healthy and young individuals. The technique is regarded as costly and the analyses of the images can be time consuming. Even though characteristic CT numbers automatically separate the different tissues, further atomisation of the determinations of depots would facilitate the post-processing.

Magnetic resonance imaging

Almost all medical imaging using MR is based on the magnetic and motional properties of the nucleus of the hydrogen atom (^1H). The nucleus, a proton, has spin and electrical charge distribution resulting in a magnetic dipole aligned with the spin axis. When hydrogen nuclei are placed in a strong static magnetic field *e.g.* in a MRI scanner, a fraction of these small magnetic dipoles will align with the magnetic field thereby collectively forming a magnetisation. The proton also has a mass, which together with the spin property results in a spin angular momentum. If the spin axis is exerted to a

torque, the spin angular momentum of the hydrogen nucleus gives rise to a precession of its spin axis. This can be observed as a precession of the magnetisation formed by the hydrogen nuclei. Precession is the same motion as the wobbling of a spinning top, whose circling axis forms the shape of a cone. The frequency of the precession, known also as the resonance frequency of the hydrogen nucleus, is directly proportional to the strength of the magnetic field. As the source of the MR-signal, the precessional motion of the nuclear magnetisation induces a current in the receiver coil of the MR scanner. For this to happen, the magnetisation must be disturbed from its alignment with the static magnetic field. A radiofrequency pulse, at the precession frequency, from the MR scanner's transmit coil causes the direction of the magnetisation from the hydrogen nuclei to flip from the aligned direction. The static magnetic field now exerts a torque on the nuclear magnetisation giving rise to its precessional motion, thereby making it observable in the receive coil as the MR signal. With time under the influence of the molecular surroundings, the hydrogen nuclei realign with the static magnetic field reforming the initial magnetisation as before the radiofrequency pulse. This longitudinal relaxation process is characterized by the time parameter T_1. The T_1 parameter, which reflects tissue properties on the cellular and molecular levels, differs considerably between different tissues. After collection of a large number of spatially encoded MR signals, an image can be reconstructed showing the distribution of MR signal intensity over the imaged tomographic section. When the repetition time between successive RF pulses is too short to complete the relaxation process, full magnetisation is not reformed. Rather, a steady state level of magnetisation, and therefore also of MR signal is established. This steady state of MR signal is dependent on repetition time, flip angle caused by the RF pulse and T_1 characteristics of the tissue (46). From two images acquired with different flip angles, *i.e.* 80° and 30°, a map of T_1 values can be calculated (47).
MRI equipments are widely spread but the technique is still regarded as a costly method for body composition purposes. The scan time can be reduced with new protocols. Manual analyses of the images are cumbersome, why automatisation is important. No ionizing radiation is imparted to subjects in MRI.

Body composition on a tissue level

Computed tomography has been used for body composition studies since the 1980:s (48-52). The technique is well suited for assessing tissue areas and volumes. It has been validated in cadaver studies (53). Different tissues have different attenuation properties, resulting in different CT numbers. These CT numbers, measured in Hounsfield Units (HU), can be used to automatically define the tissues by means of tissue specific CT number intervals, table 3 (50, 54). Tissue characterization based on characteristic CT numbers for AT and MT utilizes the whole CT number range regardless of window and level settings (55) and provides a good separation of main tissues, figure 2.

Table 3. CT number intervals for tissues

Gas	-1000	HU	–	-191	HU
Adipose tissue	-190	HU	–	-30	HU
Muscle tissue, skin, visceral organs	-29	HU	–	151	HU
Bone tissue	152	HU	–	2500	HU

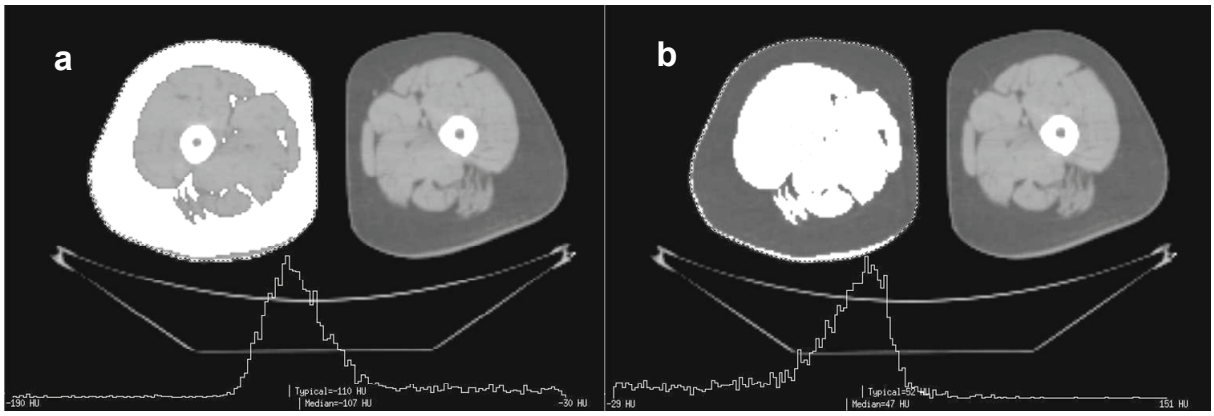

Figure 2. CT of the thigh (position 5 according to figure 7). Figure 2a shows the pixels categorized as adipose tissue (*i.e.* CT numbers from −190 to −30 HU) in white. The histogram representing these highlighted pixels is shown in the lower part of the image. Figure 2b shows the pixels categorized as muscle tissue (*i.e.* CT numbers from −29 to +151 HU) in white. The histogram representing these highlighted pixels is shown in the lower part of the image.

By defining anatomical parts of the body in each tomographic section, the depots of different tissues can be determined. For example, the subcutaneous area can be separated by delineating the border between the subcutaneous area and the peripheral muscle "border" of the abdomen, figure 3. By measuring the area of the pixels determined as adipose tissue in the subcutaneous area, the subcutaneous AT (SAT) area can be determined, figure 3.

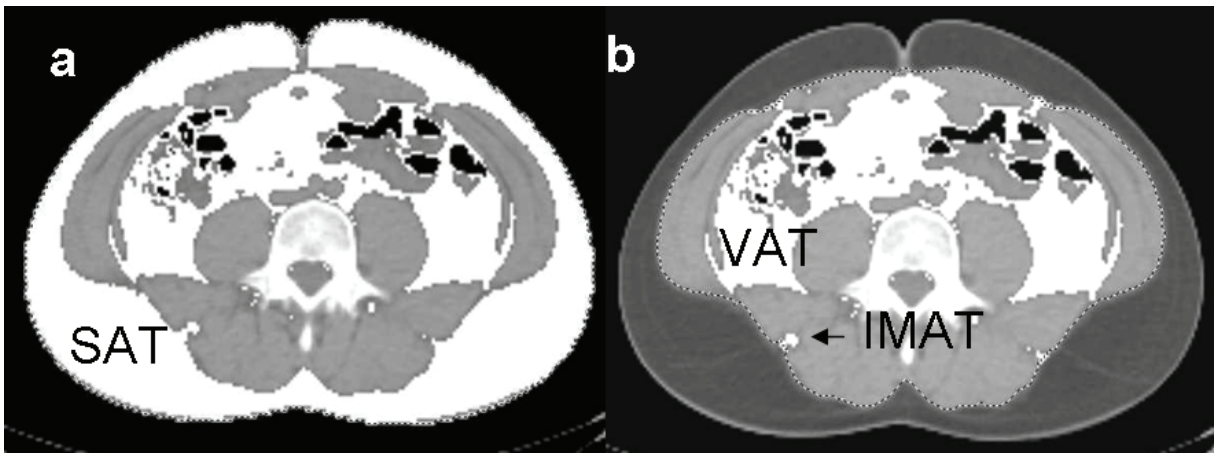

Figure 3. To asses the adipose tissue areas in the abdomen (position 11 in figure 7) all pixels categorized as adipose tissue, *i.e*. CT numbers from −190 to −30 HU, are marked (white) by the computer program as is shown in figure 3a. Figure 3b shows the semi-automatic delineation of the outer muscle border. When the area of the adipose tissue pixels in figure 3b, mainly visceral adipose tissue (VAT) and intramuscular adipose tissue (IMAT), is subtracted from the area of the pixels in figure 3a (all AT) the resulting area is the calculated subcutaneous adipose tissue (SAT) area.

If the amounts of each tissue from multiple slices are summarised, tissue volumes can be calculated. A multi compartment model of the composition of the body can then be constructed. The model described by Chowdhury and co-workers (54) divides the human body into 12 main compartments, which are further divided into a total of 21 sub-compartments. To facilitate a semi-automatic analysis of the images the description of how to determine the different tissue areas was revised and updated. Appendix A shows the updated instruction for one scan of the abdomen (Brandberg and co-workers, unpublished data). Additional compartments have also been described and Shen and co-workers proposed a classification for adipose tissue compartments in 2003 (56). The tissue compartments, *e.g*. MT and SAT, can also be divided into regional depots, *e.g.* trunk, arms, legs *etc.* The major limitation

of the CT method is the ionizing radiation imparted to the subject. To reduce the radiation dose single slice CT images and determination of tissue areas have long been used as estimates for tissue volumes. To asses skeletal MT and peripheral subcutaneous AT a slice of the thigh is commonly used. To assess VAT and SAT of the abdomen a slice of the abdomen has been used. The correlation between VAT volume and VAT by single slices is high at most levels of the abdomen and the optimal level has been discussed (49, 57). The single slice technology simplifies the analysis, which can be cumbersome, since many compartments demand manual delineation or at least visual inspection of proposed automatic delineation.

MRI has been used in body composition studies since the 1980s (58, 59). The most common technique used to assess adipose tissue by MRI is T_1 weighted images. This has been done both in single slice and whole body studies (60, 61). A limitation of conventional MRI is that the signal intensities are not homogeneous and that the signal intensity is measured in arbitrary units. It is also susceptible to artefacts in the borders between tissues.

A whole-body T_1 mapping technique has been developed in Uppsala, Sweden (47). The advantage of the technique is that it yields a better separation between AT and other tissues, see figure 4. An improved separation of tissues facilitates an automated image analysis. In paper II, this new T_1 technique was validated using the established computed tomography technique by Chowdhury and co-workers as a reference (54).

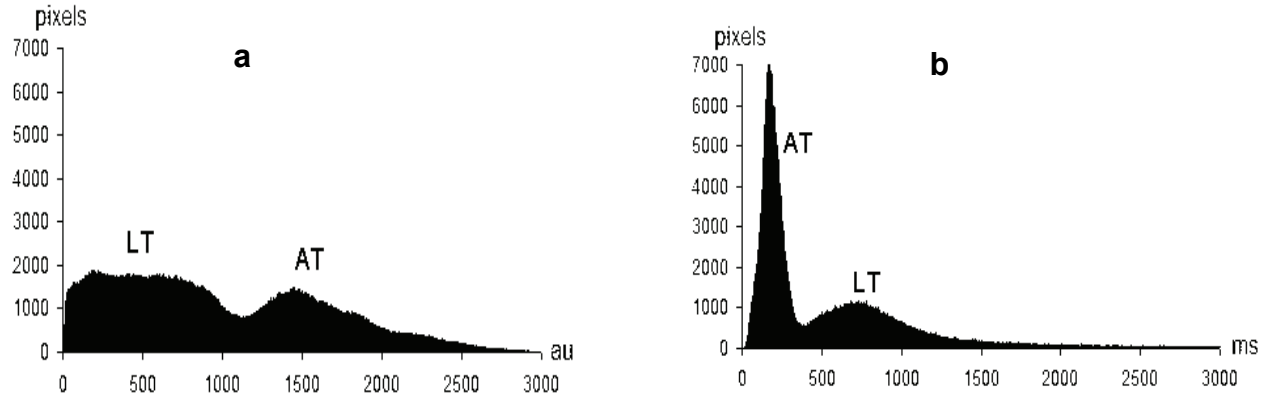

Figure 4 The histograms in **a** and **b** show the number of pixels as a function of au [arbitrary units] and msec [milliseconds] of the Flip80 and the T1-mapped whole body volumes, respectively. The histogram areas corresponding to signals from AT [adipose tissue] and LT [lean tissue] are denoted as AT and LT, respectively. There is a good AT separation in the whole-body T1 histogram.

J Magn Reson Imaging 2006;24(2):394-401

Determination of fat content in organs and tissues

Increased content of fat in liver tissue reduces the density of the liver, which lowers the attenuation of x-rays when examined by CT. Thus with increased fat content in the liver tissue a decrease in CT numbers can be recorded, figure 5. This can be used as a non-invasive tool for investigating liver fat and shows a good agreement with biochemical and histomorphometric methods (62-64). In single slice technology, a scan is performed in the mid-liver level, ~position 15, figure 7.

An altered muscle tissue (MT) composition with an increased fat content, resulting in a lowered attenuation, has been shown to be an independent marker of insulin resistance (65) and muscle strength (66).

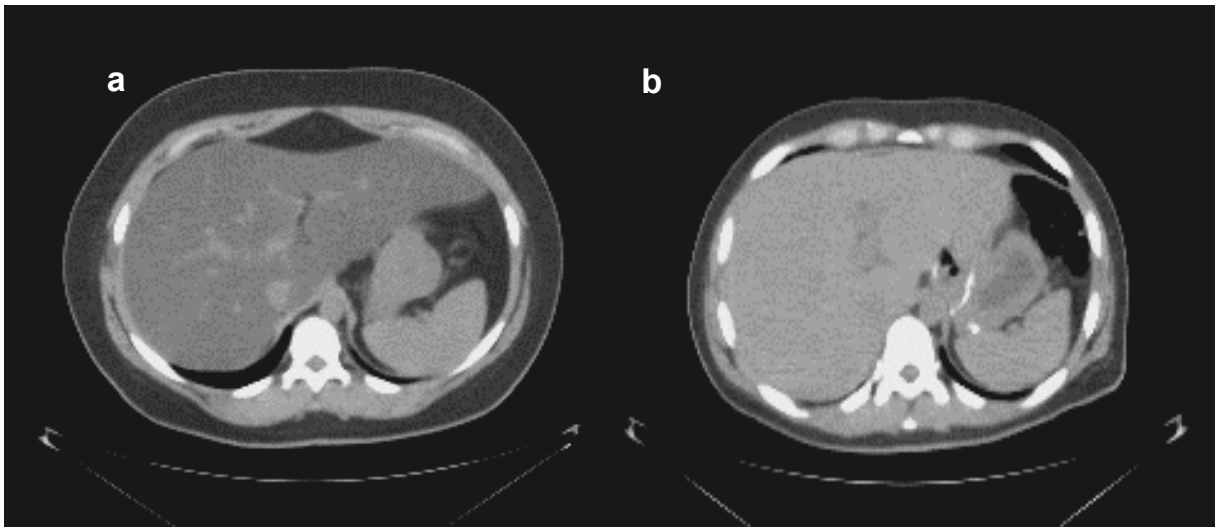

Figure 5. Figure 5a shows liver with elevated fat content. The mean CT number is −1 HU. Note that the vascular structures are detectable due to the lower density of the fatty liver relative to the vessels. Figure 5b shows the same patient after bariatric surgery. The CT number of liver tissue has increased to 53 HU.

Radiation dose, image quality, and image noise

Radiation dose is a significant issue when using CT and it represents the largest contribution to the collective dose to the population from artificial radiation sources. The use of CT is increasing as well as the relative radiation dose contribution from CT and it has been estimated to be responsible for 47 % of the total dose from medical imaging (67). CT radiation dose should be As Low As Reasonable Achievable, the ALARA principle, which implies that the specific diagnostic task and the attenuation properties of the subject must be the foundation for the selection of technique factors. The attenuation properties of the subject are related to the size, in particular to the largest diameter, which corresponds to the projection in which the x-ray beam will be most attenuated (68). Efforts to reduce radiation doses from CT in clinical medicine are therefore warranted. A basic problem related to reduction of radiation dose in CT is the inherent increase in image noise that follows a reduction in x-ray tube current. A balance between diagnostic yield and radiation dose to the patient therefore needs to be found.

Comparisons of diagnostic methods

New methods in medical imaging are often introduced despite weak evidence of their appropriateness. To match the standards set in clinical trial research, where randomized trials are the paramount study design, there is now an evolution of diagnostic study designs (69). Systematic reviews of diagnostic studies are now included in the Cochrane Library. To evaluate and characterize methods for both research and clinical applications is essential. Upon introducing a new technique, thought to be an improvement, it should be compared with the standard procedure. Methods must also be applied to reveal bias and systematic differences between equipments. This type of evaluation is an essential part of multi-centre study methodology (70). Few and very small studies have in detail investigated the imprecision of computed tomography in determination of body composition (71, 72). This is probably due to the limitations caused by the ionizing radiation dose. Using the method described in paper I it was possible to investigate this as a part of a multi-centre study (73).

Aims

I. To evaluate if the radiation dose to the subject can be substantially reduced in assessment of body composition using CT while maintaining accurate measurements of adipose tissue areas, muscle tissue areas, and muscle tissue attenuation.

II. To validate a T_1 mapping whole-body MRI method, used for assessment of body composition, by comparing it with a whole-body CT method.

III. To examine within-scanner reproducibility and between-scanner performance of CT measurements of adipose tissue areas, muscle tissue areas, and liver attenuation.

IV. To study the effects of growth hormone treatment on body composition and insulin sensitivity in postmenopausal women with abdominal obesity.

Materials and methods

Study designs and patients

Paper I describes a study that investigates whether a low radiation dose CT protocol can be used for determination of body composition. Seventeen volunteers underwent CT imaging. The subjects were recruited from a sibling-pairs study (SIB), an extension of the Swedish Obese Subjects Study (SOS). The SOS study is a longitudinal study aiming to investigate the health effects of bariatric surgery (74, 75). The focus of the SIB study is to find relationships between genotypes and phenotypes. Patients were chosen to assure a wide range of diameters for both the abdomen (31-47 cm, n=11) and the thighs (34-46 cm, n=12).

Paper II describes a study that investigates whether a proposed T1 mapping whole body MRI technique can be used for studies of body composition. Ten volunteers underwent whole body examination by MRI, CT and DXA. The subjects were members of two nuclear families of the SIB study (74, 75).

Paper III describes a study that investigates the imprecision of a single slice CT method for determination of body composition. Fifty patients were examined by CT at two study centres, Göteborg and Örebro, Sweden. The subjects were recruited from a the multi-centre study XENDOS (XENical® in the prevention of Diabetes in Obese Subjects) (73, 76). The XENDOS study was designed as a five year randomized, double-blind, placebo-controlled, prospective, multi-centre trial investigating whether orlistat (Xenical®, Hoffman-La Roche) combined with reduced-calorie diet and moderate physical exercise can prevent development of diabetes mellitus.

Paper IV describes a study of the effects of GH treatment on insulin sensitivity, visceral fat mass, and glucose tolerance in postmenopausal women with abdominal obesity were studied. The criteria for inclusion in the study were age 50–65 years, a body mass index of 25–35 kg/m^2, a waist-to-hip (W/H) ratio >0.85 and/or a sagittal diameter >21.0 cm, and a serum IGF-I concentration of between –1 and –2 SD score. The criteria for exclusion were diabetes mellitus, cardiovascular disease, claudicatio intermittens, any malignancy, and any other hormone treatment, including oestrogen replacement therapy. Forty of 145 screened women were found to be eligible for inclusion. The study was a 12-month, randomized, double-blind, and parallel group trial with subjects receiving placebo or recombinant human GH. The patient characteristics are summarized in table 4.

Table 4. Summary of patient characteristics in the studies (I-IV)

			Age (years)	Height (m)	Weight (kg)	BMI (kg/m^2)
Paper I	Female (*n* =10)	mean	43.4	1.70	84.7	29.2
		range	(23-70)	(1.63-1.78)	(57-112)	(21-40)
	Male (*n* =7)	mean	59.7	1.77	86.5	27.5
		range	(35-70)	(1.71-1.89)	(73-99)	(24-31)
Paper II	Female (*n* =6)	mean	51	1.65	76.4	27.9
		range	(38-70)	(1.61-1.71)	(59.3-113)	(22.9-38.7)
	Male (*n* =4)		57	1.80	105	32.5
			(45-71)	(1.77-1.83)	(92.4-124)	(28.8-37.1)
Paper III	Female (*n* =25)	mean	41	1.65	93.4	34.2
		range	(30-55)	(1.57-1.79)	(59.5-108)	(23.2-41.4)
	Male (*n* =25)	mean	46	1.78	101	32.0
		range	(31-61)	(1.66-1.93)	(81,6-109)	(27.2-37.5)
Paper IV	Female (*n* =20)	mean	58.2	1.67	86.0	30.5
	GH	range	(51– 63)	(1.54-1.75)	(67.0-108)	(27.0-36.9)
	Female (*n* =20)	mean	56.5	1.64	80.9	30.0
	placebo	range	(51– 63)	(1.54-1.75)	(66.5-104)	(25.3-36.7)

GH, Growth Hormone

Computed tomography systems, protocols, and scanning

For studies I-IV, CT imaging was performed using a General Electric HiSpeed Advantage CT system, at Sahlgrenska University Hospital, Centre 1. For the CT scanner comparison, in paper II, a Philips Tomoscan AVEP was used during years 0-3 at Örebro University Hospital, Centre 2. Year 4 the equipment was replaced and consequently, the ten patients examined during the last year were only evaluated regarding within centre reproducibility at centre 1.

Before study initiations, the linearity of all scanners was verified using a phantom with a variety of densities (-110.5 HU − 1375.7 HU). Throughout the studies, the scanners were calibrated with air and a water phantom on each occasion.

Two CT protocols were used in the studies. For both protocols the tube voltage (120 kV) and filtration were kept constant in order to maintain the same radiation quality in all scans. The exposure time, which was the same as scan time, was 1 s for all images. Images were reconstructed in a 256×256 pixel matrix covering a 48×48 cm^2 field of view (FOV) at Centre 1 and a 52×52 cm^2 FOV at Centre 2. The standard reconstruction algorithms in the systems were used. The first protocol was a standard clinical protocol (200mA×1s), that was used as the reference method in paper I and for the body composition assessment in paper IV. The second protocol made use of patient specific scan parameters to lower the radiation dose. This protocol was investigated in paper I (77-79) and was used for assessment of body composition in papers I, II and III, table 5. The protocol was intended to keep the expected deviation in the measured areas of adipose and muscle tissue no greater than 1 % of total tissue area measured in images acquired with standard clinical scan parameters. The investigators defined the level of acceptable deviation of 1 % in the area measured. According to calculations and *in vivo* data this condition would make it possible to reduce the radiation dose to the subject, increasing the noise level in the images up to a SD of 30 HU (78). To compensate for an increased image noise level peripherally in images from large subjects, the maximum allowed noise level was re-specified to a SD of 20 HU in the central part of the FOV for patients with a transverse diameter >35 cm in the tomographic section (77). Individual patient-specific scan parameters were chosen according to the transverse diameter of each anatomical section. The resulting doses are shown in figure 6.

Table 5. Section thickness and x ray tube current for a range of transversal diameters

Transversal diameter (cm)	31-33	34	35	36	37	38	39	40	41	42	43	44	45	46	47	Std[a]
Section thickness (mm)	1	1	1	3	3	5	5	5	10	10	10	10	10	10	10	10
Tube current (mA)	40	50	60	50	60	40	50	60	40	50	60	70	80	100	120	200
Relative effective dose (%)[b]	2	2.5	3	7.5	9	10	13	15	20	25	30	35	40	50	60	100

For all scans: exposure time 1 s, x-ray tube voltage 120 kV

[a] Reference standard clinical scan parameters

[b] The relative radiation dose from patient-specific parameters is expressed as a percentage of the radiation dose from standard clinical parameters

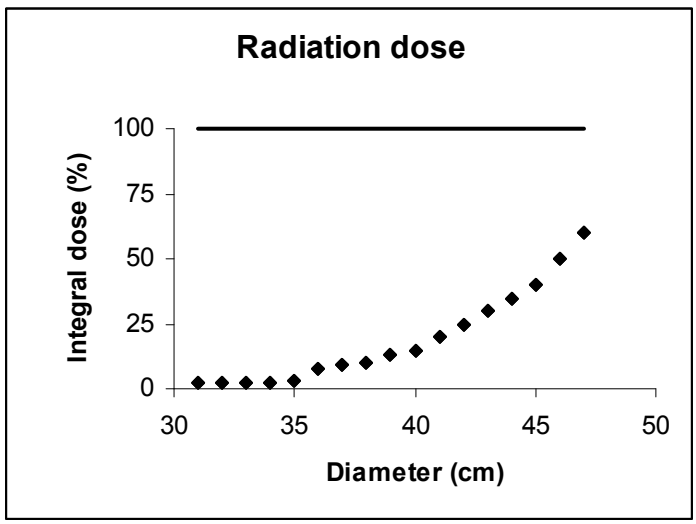

Figure 6. The solid line shows the standard radiation dose (200mA, 1s scan time, and 10mm slice thickness). The markers show the estimated relative radiation dose, using patient specific scan parameters.

In papers I and II 28 axial images were acquired from subjects in the scan positions described by Chowdhury and co-workers (54). The positions of the toes and finger-tips were also determined from the reference images resulting in a total of 30 positions, figure 7.

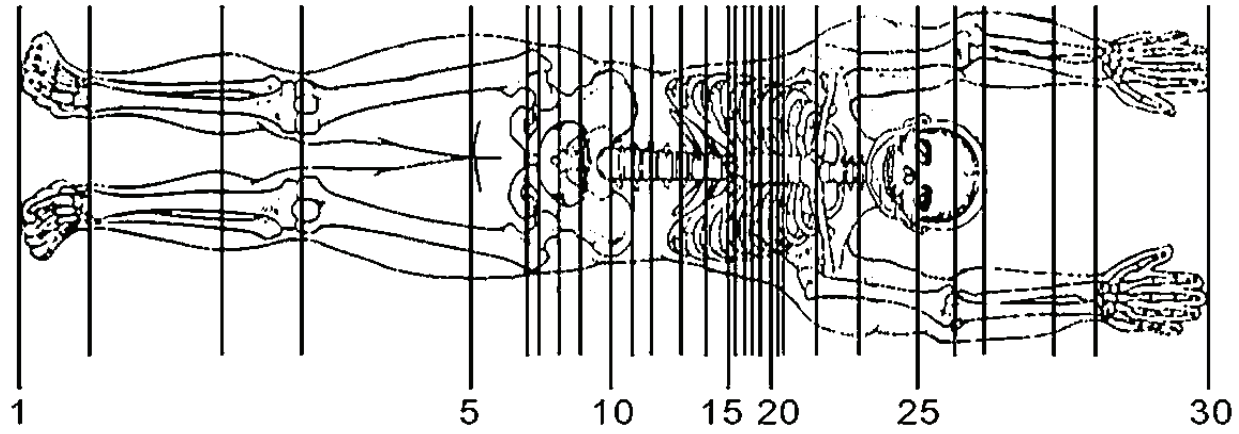

Figure 7. Slice positions of the axial images according to the 28 scan CT method (Chowdhury and co-workers). In paper I positions 5 and 11 were selected. In paper II all positions were selected for the CT examination and for the slice-wise comparisons the corresponding slice positions were selected from the MRI data set. In papers III and IV positions 5, 11 and approximately 15 (mid liver level) were selected.

In paper I, two anatomic levels that are of interest in determination of body composition were selected to compare standard and reduced integral radiation dose. The first level was of the abdomen at the top of the iliac crests, position 11 in figure 7, and the second level was in the thigh, position 5 in figure 7. Three consecutive transaxial scans were acquired at each level. The standard clinical scan parameters were used for the first scan, whereas patient-specific scan parameters for reduced dose were used for the two subsequent scans. All scans were acquired within seconds.

In paper II, two positions (1 and 30) were determined from the reference images in order to measure the total length of the subject in the supine position. Using the positions shown in figure 7, 28 axial CT images were acquired. Positions were numbered 1–30, including the 28 scans, positions 2–29, from toes to finger tips. The positions of the scans were obtained using the reference images. The subject had to be repositioned once since the maximum length of table movement was less than the length of the subject. First the scans from the ankle joint to the upper border of the iliac crest, positions 2–11, were acquired. Thereafter the subject was repositioned and the scans from the level of the third lumbar vertebrae to the wrists, positions 12–29, were acquired.

In papers III and IV three scan positions were selected from the CT reference image. The first scan was positioned in the mid-liver approximately at position 15, the second scan in the abdomen at position 11, and the third scan in the thighs at position 5 in figure 7

The within-scanner imprecision examined in paper III was determined by making two consecutive scans. The patient had to stand up between the scans and was repositioned and rescanned, repeating all steps of the examination procedure. The following day the patient was examined using an identical procedure at the other study centre. No information about the scanning procedures was transferred between centres. Four operators evaluated all images using an in-house computer program at centre 1. For within-scanner comparisons, the same operator evaluated each duplicate. Furthermore, the first image in each duplicate was independently analyzed by two operators to assess inter-observer variability.

In all studies obese subjects that did not fit into the FOV were repositioned to only exceed the FOV on one side of the body. Thus, the other side of the body, including at least 50 % of all tissue areas, was scanned and the missing parts could be compensated by doubling the areas of the contralateral half of the body.

Magnetic resonance tomography system, protocol, and scanning (II)

The contiguous whole-body MRI acquisition was performed on a Philips Gyroscan Intera 1.5 Tessla, clinical MRI scanner at Sahlgrenska University Hospital.

The protocol consisted of a spoiled T_1 weighted gradient echo sequence (47). The main scan parameters were; repetition time 177 ms, echo time 2.3 msm, FOV 530 mm, and slice thickness 8 mm. Three whole-body volumes were acquired. The first was acquired using a flip angle of 80° and was denoted as ‘‘Flip80’’. The Flip80 data were used to separate the body from surrounding air and lungs automatically. The Flip80 data were also used in the visual selection of the MR positions that best corresponded to the acquired CT positions. Scan parameters were turned off to ensure a constant MR signal scaling. The second and third whole-body volumes were acquired using flip angles of 80° and 30°. These volumes were denoted as ‘‘Flip80off’’ and ‘‘Flip30off’’, respectively, and were used in the calculation of the T_1 relaxation map (47). Owing to limitations in the hardware, repositioning of the subject was necessary to acquire a whole body volume, as previously described in the CT scanning section.

Determination of tissue areas and volumes from CT images

Tissue areas of CT examinations were determined as previously described (43, 54, 80). The area of all pixels was measured within specific CT number intervals, table 3. In paper I this evaluation was made at the CT console. In papers II-IV the acquired CT data was semi-automatically analyzed using software developed at the Department of Medicine, Göteborg University, Sweden. For details regarding the instructions for the measurements, see appendix A. AT and MT area determinations of the thigh required only minor operator dependent delineations, whereas analyses of visceral adipose tissue (VAT) and subcutaneous adipose tissue (SAT) areas of the abdomen required manual delineation. For volume calculation, the average of the areas measured in images with adjacent positions, figure 7, were multiplied with the distance between the positions according to equation 2, These inter-slice volumes were then summarised to obtain total volumes of tissues.

(Equation 2)
$$V = \sum_{i=1}^{n-1} d_i \times \frac{a_i + a_{i+1}}{2}$$

V=volume, d_i=distance between position i and $i+1$, $a_i + a_{i+1}$= sum of tissue area in position i and $i+1$

Determination of muscle tissue attenuation for comparison of CT protocols (I)

To compare the effects of the patient specific scan protocol on determination of CT numbers, the average CT numbers of muscle tissue in the thigh were measured in images acquired using clinical scan parameters and patient-specific scan parameters.

Determination of tissue areas and volumes from MR images (II)

AT was segmented from the T_1-mapped data using thresholds automatically derived from the whole-body T_1 histograms. SAT and VAT were separated manually. Using the acquired CT slices as a reference, the corresponding MRI slices were selected from the contiguous whole-body MRI volume and used in the slice-wise evaluation. In the automated T_1-mapping MRI method the adipose tissue is divided into SAT and VAT. The data for SAT includes bone marrow (BM). Accurate exclusion of BM is difficult to achieve automatically in many MRI images using this protocol. Therefore, to further assess the SAT areas measured, the BM was manually segmented in slice positions 2–9, figure 7.

Hepatic fat content (III, IV)

Hepatic fat content was measured as the average CT number within three circular regions of interest with a diameter of 20 mm placed in the dorsal aspects of the liver. Attempts were made to avoid blood vessels, artefacts, and areas of tissue inhomogeneity.

Dual energy X-ray Absorptiometry (II)

In paper II where whole body composition was assessed, whole body dual energy x-ray absorptiometry (DXA) was performed with a LUNAR DPX-L scanner with software version 1.35 and an extended analysis program for total body. Body fat (BF), lean tissue mass (LTM), bone mineral content (BMC) and body weight were assessed. Quality assurance tests were conducted on a daily basis. Based on *in vivo* double determinations the imprecision errors were 1.7 % for BF, 0.7 % for LTM, and 1.9 % for BMC (81).

Total body potassium (IV)

Total body potassium was measured by counting the emission of 1.46 MeV γ-radiation from the naturally occurring ^{40}K isotope in a highly sensitive 3-π whole-body counter with a coefficient of variation (CV) of 2.2 %. Fat-free mass (FFM) was estimated by assuming a potassium content of 62 mmol/kg FFM (42) Total body fat (BF) was then calculated as BW-FFM.

Image noise determinations (I)

In paper I, the first image was obtained while using the standard clinical parameters, the second, and the third with patient specific scan parameters, *i.e.* reduced radiation doses resulting in three images acquired at each level. Image noise was measured after subtraction of the second image from the third image. The subtraction was done to remove anatomical and tissue heterogeneity in the images to make the remaining variance of pixel-values depend mainly on the image noise. Moreover, this made it possible to evaluate image noise in areas, which had an anatomically complex composition. Clearly visible and substantial subtraction artefacts were excluded from the evaluation. Six of 29 regions of interests (ROI) were excluded from image noise evaluation due to subtraction artefacts. In the abdominal image, the noise levels were obtained as standard deviations of the CT numbers in one large elliptical ROI. The ROI was made as large as possible yet avoiding the bowel. In this way the ROI included areas with a large range of densities from fat to bone, figure 8. In the thigh image, the standard deviation of the CT numbers was obtained in one large circular ROI, made as large as possible, in each thigh. The standard deviation in each ROI was divided by √2 to correct for the increase in standard deviation caused by the subtraction.

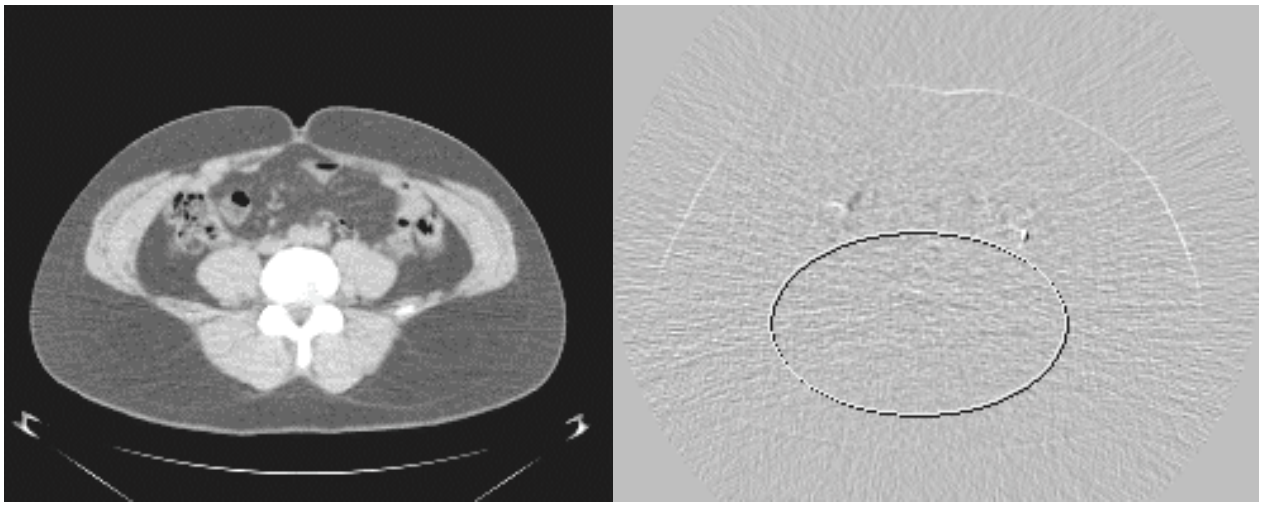

Figure 8. Figure 8a shows image obtained using reduced radiation dose and figure 8b shows the placement of the region of interest in the abdominal image after subtraction of the two images acquired with the patient specific dose parameters Due to motion artefacts in the bowel the ROI was made as large as possible yet avoiding the bowel.

Insulin sensitivity measures (IV)

In paper IV, an euglycemic hyper-insulinemic glucose clamp was performed after an overnight fast as described previously (82). An intra-venous catheter was placed in an antecubital vein for the infusion of insulin (0.12 IU/kg·min) and 20 % dextrose. A second catheter was placed in the contra-lateral arm for arterialized blood. The plasma insulin level was maintained between 150 and 250 mIU/L to suppress endogenous hepatic glucose production. Blood glucose was monitored every 10 min during the insulin infusion and every 5 min during the last 30 min,. Euglycemia was maintained (5.5 mmol/L) by infusing 20 % dextrose in variable amounts. The glucose disposal rate (GDR) was measured for 20 min in steady-state conditions, which were reached after 100 min. The mean (±SEM) insulin concentrations during steady state were 208.9 (12.4) *vs.* 219.4 (12.3) mIU/L at baseline, 210.2 (11.9) *vs.* 210.1 (8.9) mIU/L at 6 months, and 210.6 (11.0) *vs.* 210.6 (11.1) mIU/L at 12 months. All subjects performed an oral glucose tolerance test (OGTT) before the start, at 6 and 12 months, respectively, and 1 month after treatment. A standard dose of 75 g of glucose was administered, and fasting blood samples were obtained at baseline and every 30 min for 2 h. The definition criteria for normal, impaired glucose tolerance, and diabetes mellitus were based on recommendations of the American Diabetes Association (83). To eliminate any type of interference, OGTT assessments were performed one week after the glucose clamp. The homeostasis model assessment of the insulin resistance index (HOMA-IR) was estimated as described previously (84).

Biochemical assays (IV)

Blood samples were drawn in the morning after an overnight fast. The serum concentration of IGF-I was determined by a hydrochloric acid ethanol extraction radio immuno-assay (RIA) using authentic IGF-I for labelling. The SD score for IGF-I was calculated from the predicted IGF-I values, adjusted for age and sex values obtained from the normal population (85). The IGF-binding protein 3 concentration in serum was determined by RIA. The IGF binding protein 1 concentration was determined by ELISA. Serum total cholesterol and triglyceride (TG) concentrations were determined with enzymatic methods. HDL cholesterol was determined after the precipitation of apolipoprotein B (apoB)-containing lipoproteins with magnesium sulphate and dextran sulphate. The low-density lipoprotein (LDL) cholesterol concentration was calculated as described in (86). ApoB and apoA-I were determined by immunoprecipitation enhanced by polyethylene glycol at 340nm. Lipoprotein (Lp) (a) was measured by an immunoturbidinemic test. Serum insulin was determined using RIA and blood glucose was measured by the Gluco-quant method. Hemoglobin A1c was determined by HPLC, whereas C-peptide was determined by an immunoenzymetric method. Free fatty acid levels were determined using an enzymatic colorimetric method.

Statistics

The imprecision in paper I and III was estimated by means of the duplicate determinations. The standard error (*SE*) of a single determination was calculated according to equation 3.

(Equation 3)
$$SE(\%) = \frac{\sqrt{\frac{\sum d^2}{2n}}}{\bar{x}} \times 100$$

d is difference between two observations, *n* is number of paired observations, and $\bar{x}$ is the grand mean

The comparisons of standard *vs.* patient specific scan parameters in paper I and of CT scanners at Centre 1 *vs*. Centre 2, in paper III, were calculated by the same formula, regarding these measurements as duplicates in each investigation respectively. Any difference in the variances of duplicate measurements in paper III was analyzed by *F*-test. Agreement of the procedures performed with the different CT systems was assessed by ordinary linear regression analyses (OLR) in papers I-III including the 95 % confidence intervals (CI) for the slope and intercept, respectively in paper III. In the OLR, the values from images acquired with standard dose in paper I, the CT method in paper II,

and Centre 1 in paper III were used as the independent variable. For liver attenuation data, linear regression analyses were also performed using the Deming regression analysis, which in contrast to OLR allows for errors in the *x*-variable. Bland-Altman difference plots were also made in papers I-III (87). Linear correlations were studied and reported as correlation coefficients (*r*-values). Differences were investigated using the Wilcoxon signed-rank test in paper II. In paper IV all the descriptive statistical results, are presented as the mean (±SEM). The results have been analyzed on an intention-to-treat basis with the exception of the subgroup analysis of GDR and weight including only subjects who completed one year of treatment. Between-group treatment effects were analyzed using a two-way ANOVA for repeated measurements. Within-group treatment effects were estimated by one-way ANOVA or a paired Student's *t* test. Log transformation before statistical analysis was used for variables that did not have a normal distribution. An unpaired Student's *t* test was used for between-group analyses. Correlation analyses were performed using Pearson's linear regression coefficient. A two-tailed *P* value <0.05 was considered significant.

Ethics

Informed consent was obtained from each patient before entry into the studies. The studies were approved by the Ethics and Radiation Protection Committee at the University of Gothenburg and by the Medical Products Agency, Uppsala (III-IV). The estimated maximum effective radiation dose was 2 mSv.

Results

Paper I

Consequence of radiation dose reduction on tissue area determinations

The deviations in tissue area estimates of AT and MT were less than the expected maximum of 1 % of the total tissue area except in 4 out of 42 area comparisons. In these four cases, the deviations were >2 %. In the group with transverse diameters <35 cm, 3 out of 9 deviations were >1 %. For the group with transverse diameters >35 cm, only one comparison of AT area in the abdomen exceeded the expected maximum, with a deviation of 1.2 %. Area deviations for AT and MT of the abdomen are shown in figure 9. The area deviation for AT and MT of the thighs were generally smaller than in the abdomen, data not shown.

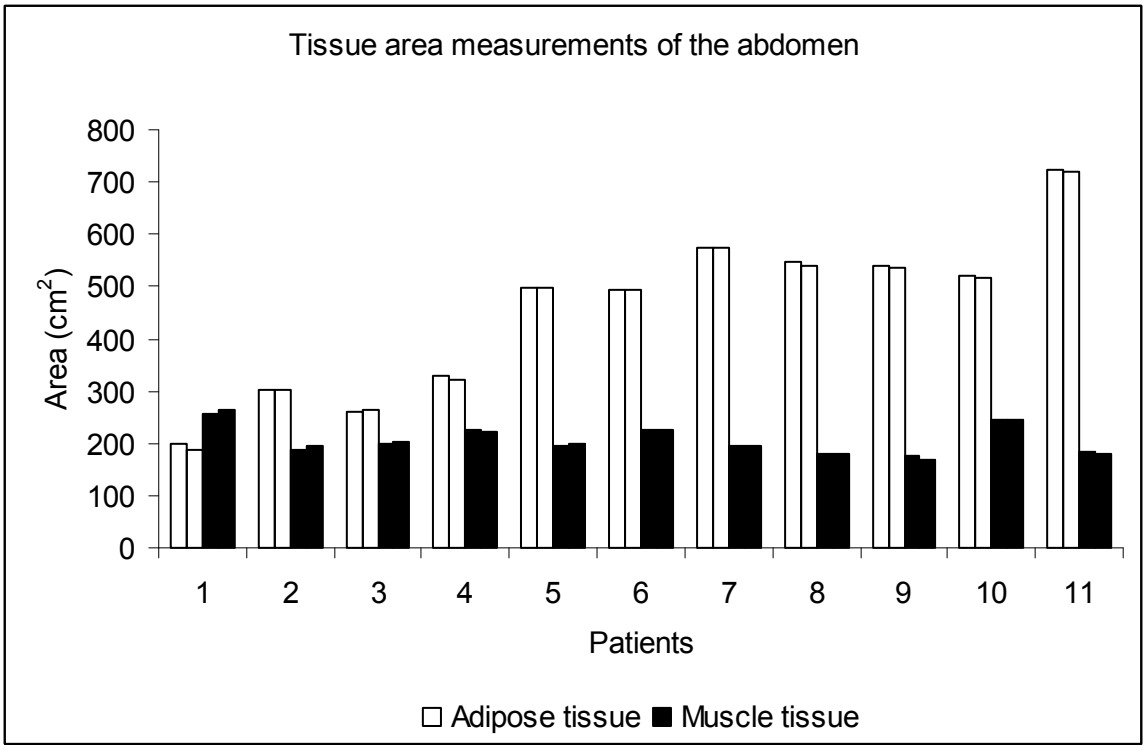

Figure 9. Comparison of areas of adipose tissue (□) and muscle tissue (■) of the abdomen determined from images acquired with clinical standard scan parameters (standard dose) as represented by the first of the two columns vs. areas determined from images acquired with patient specific scan parameters as represented by the second of the two columns (reduced radiation dose).

Measured tissue areas ranged from 140 cm^2 to 722 cm^2, and larger deviations were seen for the smallest areas. The duplicates made with patient specific parameters showed the following SE's; AT area of abdomen 0.3 %, AT area of the thigh 0.3 %, MT area of the abdomen 0.7 %, and MT area of the thigh 0.3 %.

Consequence of radiation dose reduction on mean CT number for muscle

There was no significant differences in measures of mean CT number of MT in images acquired using standard clinical parameters *vs.* images using patient-specific parameters. The difference from each comparison was plotted against the average; the mean difference was 0.28 HU its (±SD) was 0.51 HU and all individual differences were within ±1 HU and inside ±2 SD, figure 10a. The SE of the CT numbers obtained from duplicate scans with patient-specific parameters was 0.7 %. Linear regression analysis gave a slope of 0.969 (95 % CI 0.903 to 1.035), an intercept of 1.57 (-1.19 to 4.34) and r=0.995, figure 10b.

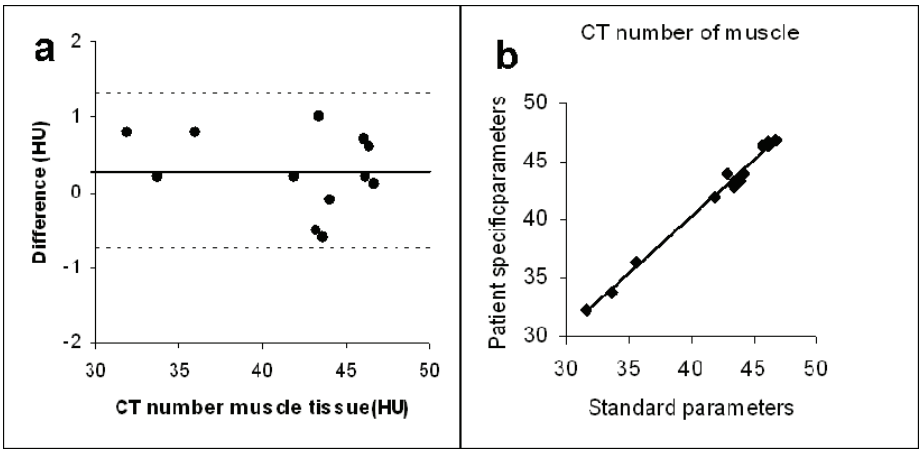

Figure 10. Comparison of mean CT numbers (HU) in muscle tissue of the thigh measured in images acquired with standard clinical parameters *vs.* patient-specific scan parameters. Differences are plotted against their means. Lines represent the mean difference and ±2 SD (standard deviations) of the mean differences (a). Linear regression line of CT number of muscle tissue acquired with patient specific scan parameters (reduced radiation dose) y-(axis) on standard parameters as the independent variable (x-axis) (b).

Image noise levels when using the patient specific scan parameters

The image noise levels remained below the specified limit of 30 HU (SD) for transverse diameters in the range of 31–35 cm, and below 20 HU (SD) for diameters in the range of 36–47 cm despite the large reductions in radiation dose when using the patient specific scan parameters. Figure 11 shows the increased image noise in the images acquired with patient specific scan parameters.

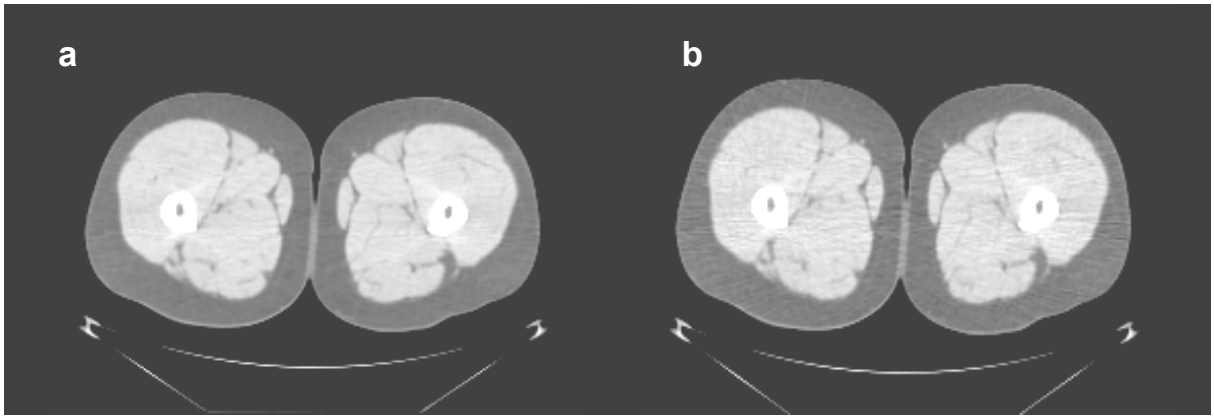

Figure 11. The image in figure 11a was acquired using standard clinical scan parameters; 120 kV, 200 mA, 1s, relative radiation dose 100 %. The image in figure 11b was acquired using patient specific scan parameters; 120 kV, 60 mA, 1s, relative radiation dose 15 %. Note the markedly higher image noise level in the image in figure 11b.

Paper II

Whole-body comparisons between MRI, CT, and DXA

The correlation coefficients between volumes measured by CT and MRI were high, for total volume r=0.998, for adipose tissue r=0.995, for SAT r=0.977, and for VAT r=0.987. Differences are recorded as mean (SD) The MRI analysis underestimated total adipose tissue volume and VAT volume by −0.61 L (1.17 L) and −0.79 L (0.75 L), respectively and overestimated SAT volumes by 2.77 L (2.41 L). The whole body fat weights estimated from the MRI analysis did not differ significantly from the whole body fat weights estimated by CT −0.56 kg (1.08 kg). DXA was found to underestimate the total fat weights compared with both CT −5.23 kg (1.71 kg) and MRI −4.67 kg (2.38 kg). The total fat weights measured by CT, MRI and DXA for the 10 subjects are given in figure 12.

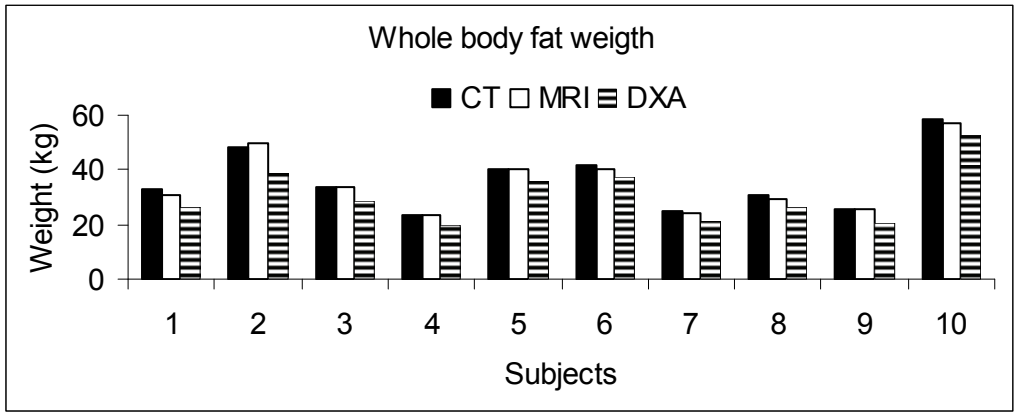

Figure 12. Whole body fat weights of the ten subjects estimated by computed tomography (CT), magnetic resonance imaging (MRI), and dual energy x-ray absorptiometry (DXA)

Slice-wise comparisons

Total slice areas

Total slice areas were often underestimated by the MRI-based method compared with CT. The absolute slice area was underestimated in 11 slice positions and overestimated in 2 slice positions. Linear regression on all absolute area differences showed a significant dependence on slice area (MRI−CT = −0.053 CT + 19.1; r=0.584, $p<0.0001$). The slice positioned at the top of the skull (position 27) was found to overestimate the area from the MRI-based method compared with CT by more than 30 cm^2 in eight of the subjects.

Subcutaneous adipose tissue areas

SAT areas were often overestimated by MRI compared with CT Significant differences were found in 19 slice positions. Slices from MRI positioned at the ankle joint, knee, pelvis, thorax and wrists were found to overestimate the SAT areas, whereas slices at the level of the third lumbar vertebra and at the level of the lower orbital border (positions 12 and 25) underestimated the SAT areas when compared with CT. Linear regression on all differences showed a dependence on the SAT area measured by CT (MRI−CT = 0.041CT + 16.7; r=0.161, p,0.0001). Significant differences were seen in five positions. After manual exclusion of bone marrow from MR images, significant differences were seen in four positions. The absolute differences in SAT areas were significantly reduced in slice positions 2, 4, 6, 7, 8, and 9 after subtraction of bone marrow. SAT was overestimated in slices at the lower border of the pubic symphysis and at the upper border of the acetabulum (positions 6 and 8) after exclusion of BM, whereas the slices at the ankle joint and calf (positions 2 and 3) were underestimated after the exclusion of BM, figure 13.

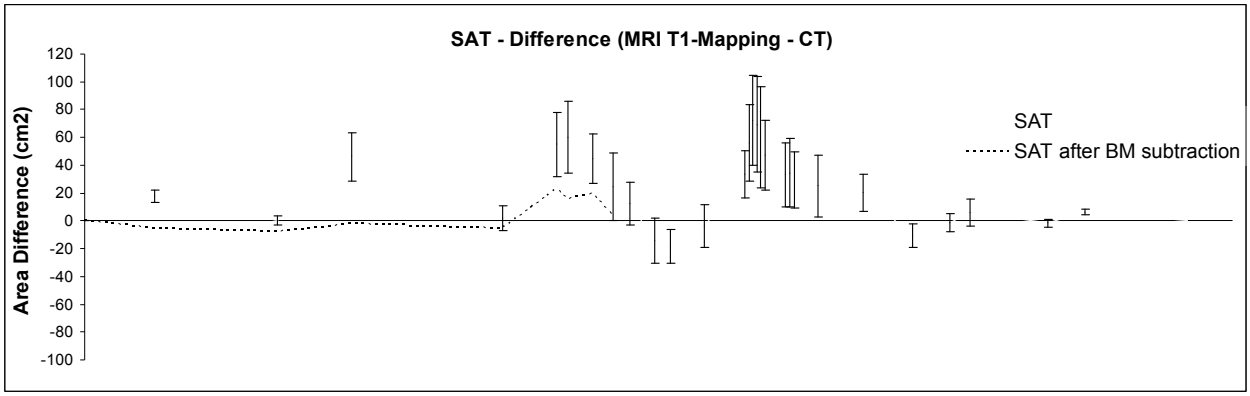

Figure 13. Slice-wise comparison of SAT differences (MRI – CT) are given as mean ± confidence interval. Dotted line represents the difference after the manual subtractions of BM from the MRI.

Visceral adipose tissue areas

VAT areas were underestimated by MRI compared with CT. Significant differences were seen in eight slice positions. Slices between the upper border of the acetabulum and at the level of the first lumbar vertebra (positions 8–13) and at the positions of the lowest point of the thoracic diaphragm and 7 mm above this position (positions 16 and 17) were underestimated by MRI compared with CT. Linear regression on all differences showed a dependence on the VAT area measured by CT (MRI −CT = −0.155CT − 0.459; r=0.575, p<0.0001). The SE for inter-operator imprecision for VAT by CT was 1.1 %. Figure 14 shows all differences in VAT area when measurements by MRI was compared with measurements by CT. Note that VAT was measured in 7-13 slices in the ten subjects. Thus, each subject contributed several data points.

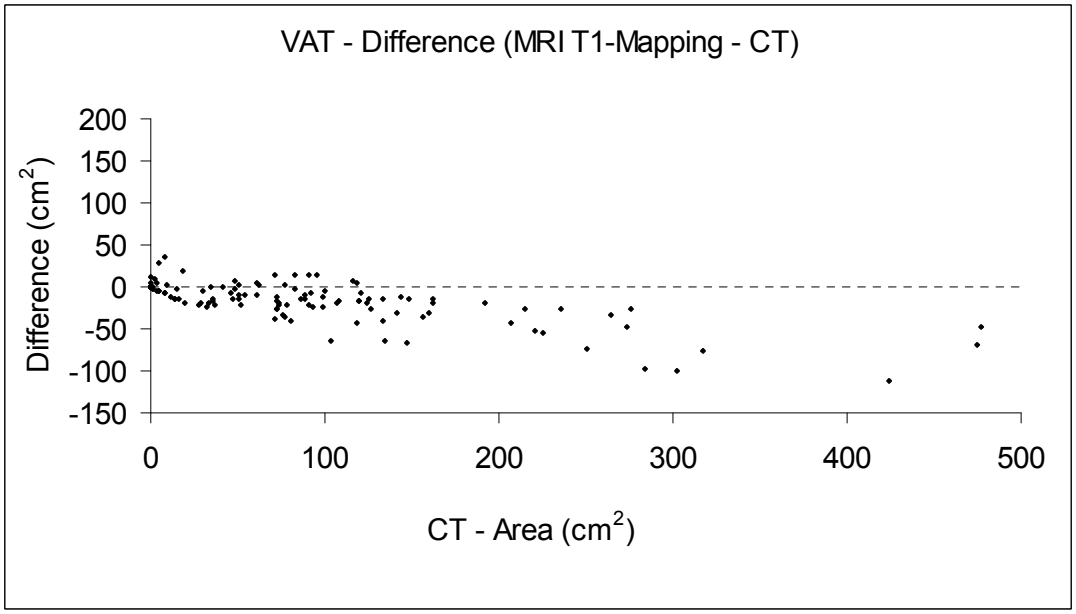

Figure 14. Slice-wise comparison of VAT area differences (MRI – CT). VAT area by CT is on the x-axis. Dotted line represents no difference (0).

In papers I, II and IV a single slice technology was used to generate a proxy for VAT volumes. The relationship between VAT area and the VAT volume by CT is shown in figure 15.

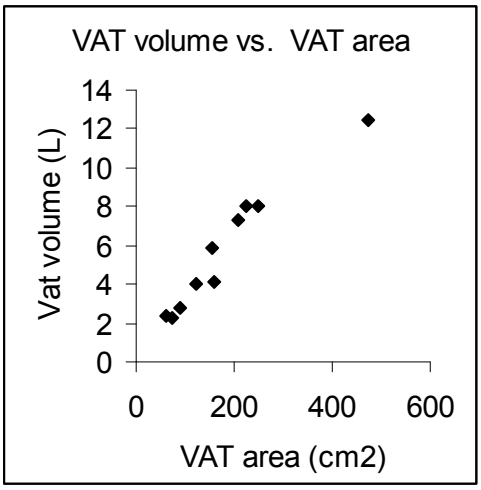

Figure 15. The relationship between visceral adipose tissue (VAT) area in a single slice and the total VAT volume by CT. The data are from the study described in paper II.

Paper III

Imprecision of body composition measurements

Table 6 shows the mean obtained from images from the two centres together with imprecision. The within-scanner SE was below 2.3 % for all within-scanners measurements except for VAT, for which SE was 6.0 % and 7.5 % for Centre 1 and Centre 2, respectively. Centre 1 showed a higher within-scanner variance for thigh SAT compared with Centre 2 ($p<0.01$, F-test). The imprecision was higher at Centre 1 and the within-scanner SE was 2.3 % as compared to 1.4 % at
Centre 2. For all other measures, there were no differences between the centres regarding the within-scanner variance. The between-scanner SE was about the same (VAT; 5.5 %) or somewhat higher than the corresponding within-scanner imprecisions, with the exception of the SE for liver CT-numbers which was 9.4 %.

Table 6. Body composition and imprecision data obtained by two CT systems

	Liver (HU)	**L4** (cm^2)			**Thigh** (cm^2)	
		SAT	VAT	MT	SAT	MT
Within-scanner Centre 1 (n=50)						
Mean	50.0	446	146	172	170	153
Mean difference (SD)	-0.3 (1.2)	-3.4 (11.9)	0.7 (12.6)	0.4 (2.3)	1.3 (5.3)	0.2 (1.6)
Reproducibility duplicates, SE (%)	2.0	2.0	6.0	1.0	2.3	0.7
Within-scanner Centre 2 (n=40)						
Mean	56.5	442	144	173	173	156
Mean difference (SD)	-0.1 (1.5)	-0.7 (8.6)	-3.5 (16.1)	0.2 (2.3)	2.2 (3.2)	-0.3 (1.9)
Reproducibility duplicates, SE (%)	1.8	1.4	7.5	0.9	1.4	0.9
Between-scanner Centre 1 vs. 2 (n=40)						
Mean difference (SD)	6.4 (3.0)	-4.2 (17.2)	-2.6 (12.0)	1.8 (4.3)	3.4 (7.5)	2.5 (2.9)
Imprecision SE (%)	9.4	2.8	5.5	1.9	3.4	1.7

Abbreviations; L4 level of the fourth lumbar vertebra; VAT visceral adipose tissue, SAT subcutaneous adipose tissue, MT muscle tissue area, SE standard error according to formula described in materials and methods section, HU Hounsfield units

Repeated readings of the same image by two operators regarding area measurements resulted in SE below 1.1 %, which should be compared with the within-scanner imprecision that was 0.7-7.5 %. Linear regression and Bland Altman difference plots of inter-operator comparisons of VAT are shown in figure 16. Repeated readings of the same image by two operators regarding CT numbers of liver tissue resulted in SE of 1.7 % and 0.1 % for Centre 1 and Centre 2, respectively. Six patients at Centre 1 and two patients at Centre 2 did not fit into the FOV.

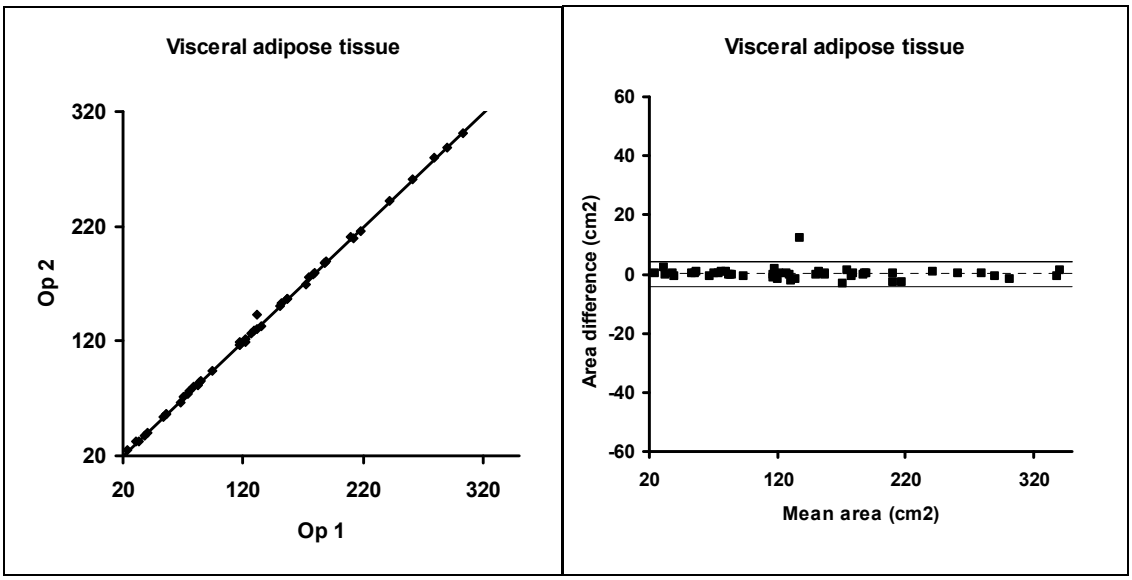

Figure 16. Results of repeated readings of the same image by two operators to evaluate the inter-operator reproducibility of visceral adipose tissue area measurements by CT.

Comparison of body composition measurements from two centres

Comparisons between the two centres were made pair-wise with regression analyses (n=40). All but one of the comparisons showed excellent agreement as the 95 % confidence intervals of the slopes and intercepts included one and zero, respectively. The exception was the equation for the measurement of liver CT numbers. The intercept of the OLR line was 5.7 HU and the 95 % CI did not include zero. Further comparisons of liver CT numbers were performed with Deming linear regression analysis. The intercept with this analysis was 4.2 HU and the 95 % CI did not include zero. Both 95 % CI of the slopes included one.

Summary of differences in area measurements (I-III)

To illustrate the magnitudes of the deviations observed under the experimental conditions described in papers I-III respectively, a single slice measurement of total adipose tissue areas was performed. The relatively small differences in total adipose tissue area induced by radiation dose reduction, the underestimation of area measures from MR images *vs*. CT images, and the differences in area measures from CT images from CT-scanners at centre 1 *vs*. 2 are shown in figure 17.

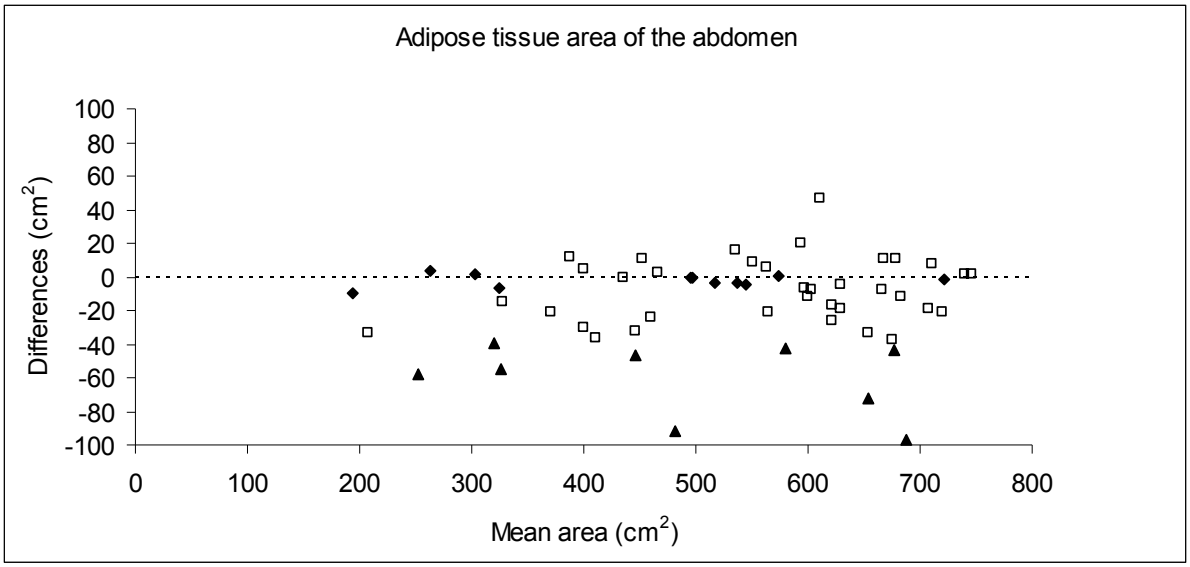

Figure 17. Summary of difference plots for total abdominal adipose tissue area of the abdomen. The differences related to mean area measured with different techniques a) patient specific *vs.* standard dose protocol (♦), paper I, b) MRI *vs.* CT protocol (▲), paper II, and c) CT system 1 *vs.* 2 (□), paper III.

Paper IV

Growth hormone treatment in postmenopausal women with abdominal obesity

Mean body weight increased in both groups, 7 of 15 women in the GH-treated group and 11 of 19 women in the placebo group gained more than 1 kg in weight, whereas the remaining women were regarded as weight stable. No changes were seen in either group or between groups for Waist circumference, sagittal diameter, or waist-to-hip ratio. MT area in the thigh increased in the GH treated group. No changes were measured in abdominal or thigh SAT area.

Changes in visceral adipose tissue and relationship to glucose disposal rate

After 12 months, GH treatment reduced VAT area, figure 18a. Although VAT area decreased after 12 months in the GH group, an increase occurred in the placebo group resulting in a significant between-treatment difference Figure 18a. Correlation analysis revealed an inverse relationship between changes in IGF-I and VAT in the GH-treated group ($r = –0.53$; $P < 0.02$). A reduction in visceral fat mass and an improvement in glucose disposal rate (GDR) occurred particularly in women who were weight stable, figure 18b. At baseline, an inverse correlation was found between VAT and CT number for liver tissue ($r = –0.49$; $P < 0.04$).

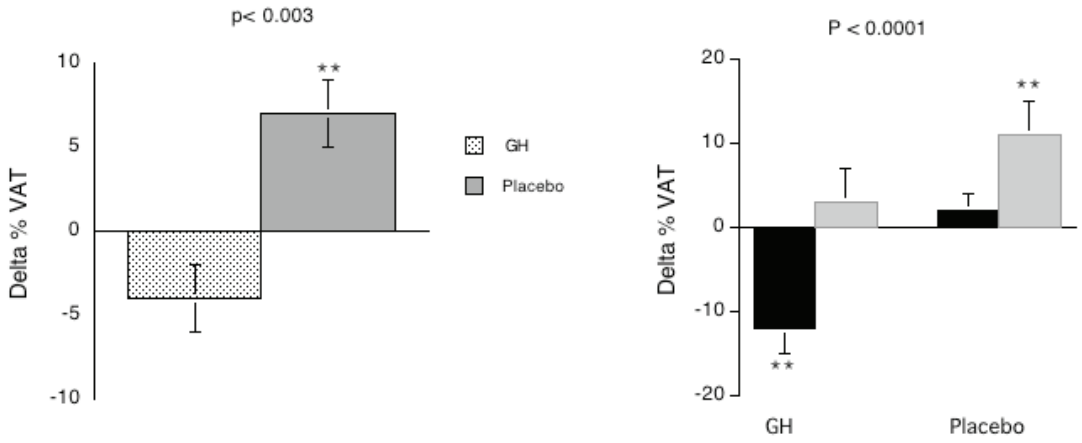

Figure 18. Change in VAT expressed as Δ percent in VAT after 12 months of GH/placebo treatment. *P* < 0.003 represents overall treatment effect analyzed using one-way ANOVA; **, *P* < 0.01 compared with baseline (a). Figure 18b Reduction in VAT expressed as Δ percent VAT from baseline to 1 yr of GH/placebo treatment with stable weight/ after 1 yr of treatment. (■) Stable weight, (GH *n*=8, Placebo *n*=8). (■) Weight gain, (GH *n*=7, Placebo *n*=11) **J Clin Endocrinol Metab 90: 1466–1474, 2005**

Changes in hepatic fat content and relationship to GDR

The percentage change between baseline and 12 months of treatment the CT number for liver tissue showed a positive linear correlation with the percentage change of GDR (r= 0.65, P <0.01) in the GH-treated group. The reduction in hepatic fat content (increased CT numbers) and an improvement of GDR was seen among the GH-treated women who had a stable weight or experienced a weight reduction throughout the study period, figure 19. Serum aspartate aminotransferase and alanine aminotransferase activities were inversely correlated with increased CT number for liver tissue in the GH-treated group (r = –0.84, P < 0001; and r = –0.81, P < 0.0001, respectively).

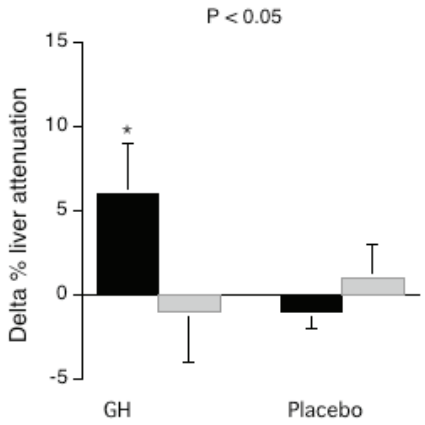

Figure 19. Reduction in hepatic fat content expressed as Δ percent in liver attenuation in GH/placebo treatment with stable weight/weight gainafter 1yr of treatment. (■) Stable weight, (GH *n*=8, Placebo *n*=8). (■) Weight gain, (GH *n*=7, placebo *n*=11) **J Clin Endocrinol Metab 90: 1466–1474, 2005**

Insulin sensitivity and glucose metabolism

GDR was similar in both groups at baseline. Between-group analysis did not reveal any difference in GDR after one year of treatment with GH. Within-group analyses showed slight initial decrease in GDR at six months, followed by a significant increase at 12 months in the GH-treated group. No changes were seen in the placebo group. In women with baseline values below the median for the group (median=8.4 mg/kg·min) the increase in GDR was more marked.

GH dose and serum IGF-I

The mean maintenance dose of GH was 0.51 (0.05) mg/day. The baseline mean serum IGF-I concentration was 121 ± 24 μg/L in the GH group and 105 ± 31 μg/L in the placebo group. In response to GH treatment the serum IGF-I increased in the GH group after six months, with no further change at 12 months.

Descriptive statistics for postmenopausal women with abdominal obesity

The variables defining the inclusion criteria regarding abdominal obesity in this study, *i.e.* BMI of 25–35 kg/m^2 and in addition a WHR >0.85 and/or a sagittal diameter >21.0 cm is compared with VAT area by CT at baseline, figure 20. The relationship between VAT area and circumference is also shown.

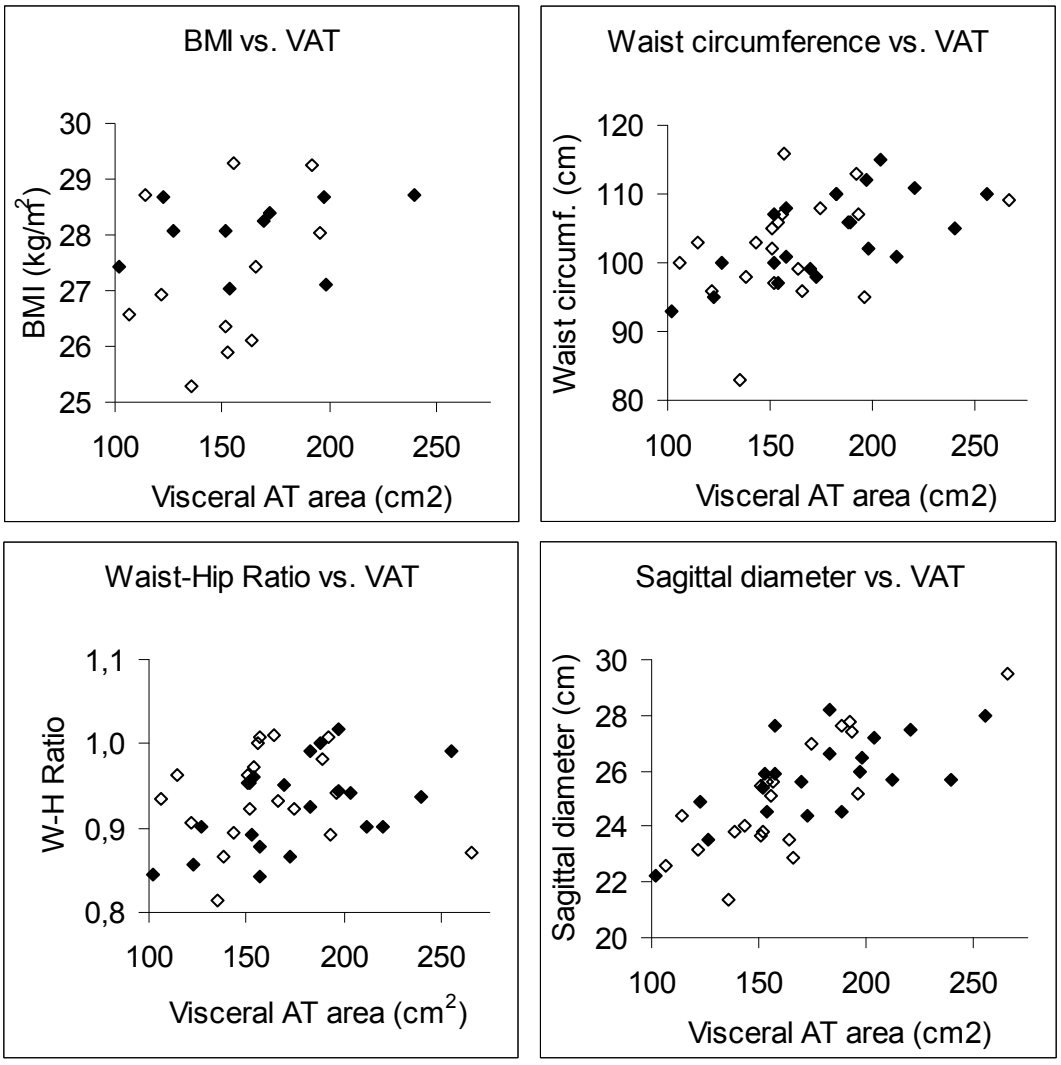

Figure 20. Filled markers represent women who received GH treatment in the study and unfilled markers received placebo The figure illustrates the relationship between visceral adipose tissue area (VAT) by CT and BMI, VAT and waist circumference, VAT and waist-hip-ratio, and VAT and sagittal diameter.

Discussion

CT and MRI in body composition

CT determination of body composition has several advantages. Image acquisition time is short and CT numbers are given on a fixed scale directly corresponding to tissue property, mainly tissue density. This makes tissue characterization robust. CT also has a high geometrical resolution and few artefacts. The analysis of the CT images can be made semi-automatically rendering a large number of tissue compartments and regions. Further, the equipment is widespread and the costs are lower as compared to magnetic resonance imaging but may still be regarded as expensive. Ionizing radiation received by the subject is the major disadvantage of the CT technique. The T_1 mapping MRI technique described in this thesis yields a better separation of adipose tissue than standard T_1 protocols (47). The technique can solve the problems with the inhomogeneous signal intensities in standard T_1 weighted imaging. The new method was validated with the CT technique as a reference and can be used in an almost fully automated post-processing. The technique has great potential for research applications including whole body studies in children and adolescents, for whom radiation protection issues are of greater importance than for older individuals.

Radiation dose, image quality, and image noise (Paper I)

The CT scan is defined by several technique factors, which influence the radiation dose to the subject as well as the qualities of the produced image. Such technique factors are x-ray tube voltage, x-ray tube current and its modulation to object size and object properties, x-ray beam filtration, x-ray beam collimation, detector efficiency, section thickness, reconstruction matrix and field of view, and reconstruction filter. The reconstruction filter determines the balance between spatial resolution and image noise when reconstructing the projection dataset to an image. If no subject specific optimization is done, differences in the size and density of the examined object will generate a large variation in detector irradiation. This causes a corresponding variation in image noise (68). The most common way to determine the radiation dose required for a specific task is to define what image quality is necessary and then record the corresponding image noise level. Then, the CT scan is individually optimized so that the patient should not receive a radiation dose that is larger than necessary, still limiting image noise to the specified level. Usually image quality requirements are higher for small subjects than for large ones and thus image noise levels may need to be lower for small subjects. When high image quality is not necessary, there is a large potential for dose reduction (77). Thus, the radiation dose can be reduced for a large number of patients by selecting scan parameters according to their body size, thereby creating more equal image noise levels for different sizes and over various parts of the body. In a phantom study designed to produce a technique chart for paediatric imaging by Boone and co-workers (88), phantoms with diameters between 12 cm and 35 cm were examined. They showed that a 20 cm phantom required only 4.5 % of the mAs required for a 35 cm phantom to achieve the same noise level. In our studies applied in patients, we demonstrated a corresponding reduction in radiation dose with a similar change in largest patient diameter. In paper I, the size of the patient was defined as the largest transverse diameter, as the x-ray beam would be attenuated the most in the projection along this diameter. The shape of the tomographic section is also an important factor when adapting technique factors for constant image quality. Kalender et al, utilized the fact that the largest contribution to image noise comes from projections with the largest attenuation through the tomographic section and achieved a substantial radiation dose reduction without a corresponding loss in image quality (89, 90). In addition, the largest diameter of the subject is easy to determine and should be an accurate estimation of the highest attenuation through the tomographic section. Different body size parameters have been tried for individual dose adaptation, *i.e.* body weight or body circumference (91). In a study on dose reductions in abdominal imaging, the scan parameters were adjusted to body weight (68). However, it is obvious that patients with the same weight can show a large variation in size of the tomographic section. In the method described in paper I, the radiation dose was reduced to achieve a specific and constant image quality, and thus noise level. Dose reduction achieved by automatic exposure control can further reduce the radiation dose while maintaining the same image quality (89, 90). Although the work in paper I was performed using a

single-slice scanner, the same principles for dose reduction also apply to multi-slice scanners. However, if only separated single sections need to be examined, a multi-slice CT might, depending on beam collimation and scanning mode (axial or helical), expose the subject to a larger radiation dose. Therefore, multi-slice CT should be operated in axial single-slice mode for body composition measurements in separated single sections to attain the radiation dose reduction described in this work. Routine CT examinations, in which each patient is scanned with the same scan parameters, show a large variation in the number of photons reaching the detector owing to variations in patient size, resulting in a correspondingly large variation in image noise. Instead, the adequate outcome of a specific CT examination should be to produce the same image quality for each patient, regardless of size. One can also argue that, for patients with little body fat, a slightly increased image quality may be required for certain diagnostic tasks, as lack of a surrounding fat layer makes tissues and internal organs more difficult to delineate. Nevertheless, a substantially lower effective radiation dose should be sufficient for patients with small diameters.
Image noise values were measured after subtraction of two images obtained in identical cross sectional scan position, with identical patient-specific parameters, which should make the variance depend only on the image noise and not on anatomy or heterogeneities in the tissues examined. In contrast, the SD of CT numbers measured in ‘‘homogeneous’’ tissue is composed of both image noise and tissue heterogeneity. Therefore, the SD measured after subtraction is generally lower. The subtraction of two identical scans makes it possible to evaluate image noise in areas that have an anatomically complex composition, *e.g.* the central parts of the abdomen. In all cases, the image noise was below the predefined limits of 20 HU (SD) and 30 HU (SD) for patients with large and small diameters, respectively (77).

Methodological considerations in comparative studies (Papers I-III)

In paper I, a new method with a lower radiation dose was compared with an established method using standard radiation dose. In paper II, an MRI method was compared with a CT method. In paper III, two different equipments were compared to assess the imprecision for each equipment as well as to reveal any bias between the equipments.

Evaluation of imprecision

It is important to control the pre-analytic variables and have a rigid standardization of the conditions under which imaging for body composition is performed. Examples of patient related variables that may need to be standardised are time of day, timing and amount of food intake, and recent physical exercise. Care should be taken to relate the pre-analytical variables to the aim of the investigation. In paper I, where a low dose protocol was to be evaluated, the scans were performed within seconds. On the other hand in the evaluation of two CT-scanners used in a multi-centre study, paper III, the subjects had to leave the CT table and repeat all the steps of the scanning procedure.
The imprecision is a measure of the closeness of a series of measurements of the same material (92). Investigating the imprecision is usually one of the first steps in a method comparison study. It can be expressed as the standard deviation (SD) or as coefficient of variation (CV), which is the SD divided by the mean, usually expressed as a percentage. Since a large number of repeated measurements is required to calculate the CV, this can be difficult to achieve in patient studies. Thus, it would not have been reasonable to make more than duplicate measurements at the two centres because of the potential hazards of ionizing radiation, paper III. An alternative way to obtain an estimate of the imprecision is to make duplicate measurements and calculate the SD, *i.e.* the sum of squares of the differences between the duplicates divided by twice the number of pairs, and the SD is its square root (92). This can be related to the grand mean, which is the mean of all duplicate measurements, to get a standard error of the grand mean. This can be expressed as a percentage, see equation 3, which expresses the imprecision for the sample used for the measurements. In the studies in paper I and III the imprecision was generally low. Such calculations were performed for the evaluation of any differences in the measurements of CT numbers for liver in paper III, further discussed in “Comparison of CT number of muscle and liver tissue”.

Evaluation of agreement

In papers I-III tissue areas, tissue volumes, and CT numbers were compared. These are all quantitative data and thus parametric statistical methods might be possible to apply, provided that the values are normally distributed. That this is the case can be tested by a normality test (93). This should be true for the material as a whole or at least for the differences of the compared material as in paper III.

There are two types of bias between methods, systematic and proportional bias. A combination of the two is also possible. Bias can be revealed and illustrated by Bland Altman difference plots as was made in papers I and III (87). The differences for each paired observation by method A and method B, respectively, are plotted on the *y*-axis and the means of the two methods on the *x*-axis. A confidence interval can be calculated for the resulting difference. This analysis was performed for several measurements in papers I-III and revealed the bias more evidently than an ordinary linear regression (OLR) plot based on least square calculations (87). OLR defines a straight line between an independent *x* and a dependent *y* variable assuming that the SD of the *y* values is normally distributed for each value of *x*. The method assumes no error in the *x* variable. The test gives a value of the slope and the intercept. The null hypotheses for the intercept and for the slope are that they do not differ from zero and one, respectively. The assumption that the independent variable *x* is determined without error is a disadvantage and the effect of such errors results in a slope that is smaller and an intercept that is greater than the true values. These differences become greater the smaller the range of measured values. This is problematic if an equation is to be constructed to pool the data from the different methods as in the multicenter study described in paper III (73, 76). Calculations of regression lines were parts of the methodological investigations in papers I-III. The correlation coefficient *r* describes how close the slopes of *x* on *y* and *y* on *x* agree. If the points lie on a straight line, *r* is 1.0 regardless of the slope. The probability for *r* can be calculated to give the statistical strength of association. For method comparison it would be surprising if there was no statistical correlation between method A and method B, therefore this operation is irrelevant in such a case (87), *i.e.* papers I-III. However, in the assessment of the slope and the intercept, the correlation between methods needs to be high, one proposed level is at $r>0.995$ when based on a wide range of data. In a case where the range of data is less than one decade, *i.e.* the range is from the minimum value to ten times the minimum value, an *r* value >0.975 is considered sufficient (94).

Due to the limitations of the OLR method, there are other linear regression models that assume errors in both *x* and *y*, which can be used. The Deming regression model minimizes the deviations from the regression line taking errors in both *x* and *y* into account (94). As it uses the imprecision of both methods, duplicate measurements are needed. As OLR, the Deming regression is highly influenced by data pairs that are higher or lower than the majority of data. In our study of two CT scanners, paper III, it cannot be assumed that any of the scanners is without error. Since the narrow confidence intervals of the slope and intercept from OLR included 1 and 0, respectively and the agreement was good, further analyses were unnecessary except in the case of CT numbers for liver. If an equation was to be constructed, the Deming method would be preferred from a statistical point of view. In all method comparisons there is a need to define agreement as the problem is one of estimation rather than hypothesis testing (87). The statistical methods applied are used to assist in the decision of agreement. The method comparisons made in papers I-III demonstrated the assessments of both agreement and bias, which are further discussed in following sections.

Comparisons of tissue areas and volumes (Papers I-III)

Classification of tissues

Many causes contribute to differences in volume and area measurements with imaging methods. As is seen in paper I, a lower radiation dose increases the image noise. This leads to an increased distribution of CT numbers in the histogram of the image as the CT numbers for different tissues will have a larger spread. The result is lower peaks for AT and MT. Due to the increased spread of CT numbers with reduced radiation dose, pixels from the tissue of interest may fall outside its specified segmentation interval. In this way, a broad peak in the histogram can influence the tissue categorization of pixels. This will contribute to a difference in area or volume determinations as

compared to measurements in an image with a standard radiation dose. In addition, the proportions of the areas influence this error due to partial volume effect (78). The new MRI T_1 mapping technique, paper II, had an improved histogram compared with standard T_1 weighted MRI techniques, figure 4. The pixel value is given as a specific T_1 relaxation time for the voxel, measured in milliseconds. Since the pixel values are given on the fixed scale of T_1 relaxation times they are comparable between scans in the same patient as well as between patients. This is analogous to CT numbers, which are given on the fixed Hounsfield scale. The reduced variation of pixel values from inhomogeneous tissue is one of the reasons for the reduced number of ambiguous pixels in the MRI images and would hence reduce the number of misclassified pixels (47).

Differences in classification of tissues occurred when comparing MRI and CT. VAT was underestimated by MRI as compared with CT, paper II. One possible explanation for this is that CT pixels partially containing intestinal gas and partially containing intestinal content will be categorized as adipose tissue. A previous study has shown that the intestinal content might contribute ~20 % to the VAT area measured by single-slice CT (95). There was no evident effect of gas in the intestines in MRI but gas is known to lower signal intensity due to susceptibility effects. Thus, intestinal content could possibly affect the results from the separate modalities differently.

The MRI method only separates total AT, SAT, and VAT from other tissues. In the MRI method, SAT was defined as all adipose tissue that is not VAT. In the CT method, adipose tissue is usually divided into SAT, IMAT, VAT, and white bone marrow. From the areas recorded as SAT_{CT} the areas of IMAT, VAT, and white bone marrow are subtracted. This could be part of the explanation that the MRI method was frequently seen to overestimate the SAT areas measured especially in the knees, pelvis and thorax, *i.e.* in slices containing relatively large amounts of bone marrow. The differences were smaller when bone marrow was manually subtracted also in the MRI, see figure 13.

In paper II there was a slice-wise comparison between the CT and MRI technique. However, for the whole-body comparisons of tissue volumes the contiguous 8 mm slices of the MRI was compared to the 28 slice positions in the CT model. Thus, this comparison should be regarded as a comparison of the techniques as a whole in contrast to the more detailed, but on a whole body level, less valid comparison of the techniques slice by slice.

The MRI method is adapted for automated post-processing (47) but in the present study the separation between VAT and SAT was made manually. In a work by Kullberg and co-workers an automated separation between SAT and VAT has been described (96). On the other hand, the CT images are evaluated by a semi-automatic method and the evaluation of a whole CT data set is done in ~2 hours. However, more tissue compartments are separated with the CT-method, described by Chowdhury and co-workers (54), the most important being SAT, IMAT, VAT MT and visceral organs (and white bone marrow for exclusion). It also records CT numbers for liver and muscle tissue. For an example of the details, see the descriptions in Appendix A. In conclusion, there are differences between the CT and MRI methods but they are generally small. Both methods are possible to use for body composition measures but the described MR method mainly determines adipose tissue depots.

Differences due to repositioning and motion

In paper I, where repeated scans were acquired within seconds without repositioning, subtraction artefacts caused by minor motion of the subject was seen. Duplicates as acquired in paper III, differed in slice position, due to the repositioning of the patient between the scans. Furthermore, for the images of the abdomen differences due to peristaltic movements and the patient's ability to reproduce the same respiratory status are added. Both CT and MRI scans of the abdomen are sensitive to peristaltic movements, especially when single slice techniques are used. Further, even if there is a perfect match of abdominal level with reference to the spine, the position of the bowel and mesenteric fat can be different between occasions in longitudinal studies. It is also difficult for patients to reproduce the same respiratory status between occasions. The MRI sequence was sensitive to motion artefacts from the heart, which led to an underestimation of lung volumes as compared to CT. To limit the problems with repositioning specially trained staff should perform the positioning of the patients. Training breath-hold technique is well known to improve the subjects' ability to repeat the same respiratory

status. However, in conclusion, the influence of motion and repositioning technique in studies I-III were generally small.

Limitations in equipments

In paper II the shapes of the CT and MRI table-tops differed slightly. In cases where patients that did not fit for the FOV (Papers II and III), the results of the measurements of the contralateral half of the tomographic section was used as a substitute for the missing area and it increased the variance of the measurements from these patients. This contributed to the higher variance seen at Centre 1 for the measurements of SAT area of the thigh in paper III. Further, when the whole subject does not fit in the FOV in CT it also induces an artefact in the reconstructed image in the form of shifted CT numbers. The shifted CT numbers can also contribute to differences in classification of pixels according to the scale of characteristic CT numbers for tissues, table 3. Another possible cause for differences in area measurements is the tomographic section thickness. In paper I, the slice thickness had to be decreased in order to achieve the lowest radiation doses, since it was not possible to decrease the tube current below 40 mA on the CT equipment used. The slice thickness influences the partial volume effect. MRI is more sensitive to the presence of metal than CT and the presence of dental metal in one subject gave artefacts that are more pronounced in MRI. Larger gantries are developed for both CT and MRI. In new scanners there is an increased distance in table top movement as compared with older ones. This would improve the methods and make it possible to examine larger subjects and to perform whole-body examinations without repositioning.

Comparisons of CT number of muscle and liver tissue (papers I and III)

The large reduction in radiation dose, paper I, did not affect the mean CT number in MT (mean difference 0.28 HU; SD±0.51 HU). Goodpaster et al. (65) showed that an increased fat content in muscles, estimated by decreasing CT numbers, is related to insulin resistance. In that study, duplicate scans with unchanged scan parameters were performed for six patients. They reported differences that were comparable to the differences in our study when CT numbers were measured in images obtained with standard clinical parameters *vs*. scan parameters for reduced radiation dose. Changes in muscle CT numbers over time have been studied in patients with acromegaly before and after adenomectomy, where the mean muscle CT number decreased from 53 HU to 48.5 HU (36). In view of these earlier results, the proposed scheme, with patient-specific scan parameters to reduce the radiation dose should be sufficient to evaluate mean CT numbers of tissues accurately. In paper III the within-scanner imprecision was small for CT numbers of liver tissue at both centres. However, between-scanners performance was also studied regarding CT number measurements of liver tissue. Comparisons were made pair-wise with regression analyses. The intercept was +4.2 HU, using the Deming linear regression, and the CI did not include zero. The CI for the slope included one and the correlation was 0.972. Thus, the investigation revealed a systematic bias in measurements of liver CT numbers. This has to be taken into consideration and makes it problematic to define scanner independent thresholds *e.g.* for fatty liver assessment. In clinical practice one of the most commonly used diagnostic decisions based on a threshold for CT numbers is the one for adrenal lesions. A high lipid content (<10 HU) strongly indicates that the adrenal lesion is benign while a higher HU value, thus indicating less lipid, suggests that the lesion might be malignant. From an evaluation of attenuation values of adrenal tumours mean differences up to 4.6 HU (range 1.7-7.0 HU) between scanners have been reported (97, 98). The magnitude of the difference is comparable to the one found in our study. These differences could be referred to individual scanner performance including image reconstruction algorithms.

DXA (Paper II)

Our study confirms that reliable results from DXA can be difficult to obtain in subjects with a body weight over ≈100 kg (99). DXA underestimated fat weight especially in the largest subjects. The three heaviest subjects exceeded the FOV, leading to an underestimation. Large obese subjects (>120 kg) have previously been reported to give false results (99, 100). The number of pixels that are determined to contain bone is increased with increased fat in the measured FOV, which could influence the calculated amount of body fat by DXA (101). Differences in results obtained by two Lunar DPX-L

machines, identical according to the manufacturer, have been reported as well as differences due to machine type and manufacturers (81, 100, 102). Advantages with DXA are that the within-scanner reproducibility of DXA is high and the radiation dose received by the subject is low. The scanning as well as the evaluation is performed quickly. In contrast to most CT measurements, interpretation of results from different DXA scanners in one study, cross sectional or longitudinal, may be difficult (81).

Effect of GH treatment on body composition (Paper IV)

Assessments of body composition by CT scan showed a clear reduction in VAT and an increased amount of thigh muscle mass in the GH-treated postmenopausal women with abdominal adiposity. In a similar study involving middle-aged men with abdominal obesity who received GH treatment for 9 months, abdominal SAT decreased (33). This was not seen in our study, suggesting that postmenopausal women are less responsive to the lipolytic effect of GH in the subcutaneous fat depots (103, 104). Data comparing *in vitro* abdominal and gluteal subcutaneous adipose tissue metabolism suggest that the menopausal status is associated with changes in AT metabolism that predispose to lower lipolysis and higher activity by lipoprotein lipase, in abdominal and gluteal SAT (105). The results in paper IV suggest major responsiveness by VAT compared with SAT, which is in agreement with previous data in GH-deficient subjects (106, 107).

The relative change between baseline and 12 months of the CT number for liver tissue showed a positive linear correlation with the relative change of glucose disposal rate (r= 0.65, $P < 0.01$) in the GH-treated group. There are data that suggest that an increase in CT number could be caused by an increase in glycogen in the liver (108). However, this would most likely have been linked to an increased insulin resistance and our data suggest that, on the contrary, it is linked to an improvement in glucose metabolism with a higher GDR. The correlation found between changes in GDR and CT number of liver in combination with a reduction of VAT and cholesterol (total and LDL cholesterol) in the GH treated group suggest that the improvement of some of the features of the metabolic syndrome was associated with a reduction in hepatic fat content. This is consistent with previous observations showing that the degree of insulin sensitivity is strongly linked to CT number of liver and hepatic fat content (109, 110). VAT has a direct connection to the liver through the portal vein. Visceral obesity probably increases the delivery of fatty acids to the liver, contributing to hepatic fat accumulation. GH treatment, with its strong lipolytic action on VAT, might therefore induce or aggravate non-alcoholic fatty liver disease. This could be an early effect however, our data suggest that 12 months of treatment reduces the hepatic fat content as a result of reduced VAT and/or an increase in the output of fat from the liver by enhanced VLDL production and secretion (111) or increased biliary lipid output (112). These data therefore support the hypothesis that the improvement in insulin sensitivity exhibited might be mediated by a reduction in hepatic fat content. A more effective peripheral glucose use by the increase in muscle mass might also have contributed to the improvement in insulin sensitivity. However, the positive correlation between liver attenuation and GDR, but not between muscle mass and GDR, suggests that the reduction in hepatic fat content was more important. The correlation analysis and subgroup analyses performed suggest that women who had a stable weight or lost weight during the study were more responsive to the metabolic effects of GH than women who gained weight during the trial, figures 18 and 19. GH treatment may therefore have an additive beneficial effect over and above the weight loss obtained by modifications in caloric intake or any other form of lifestyle interventions.

In subjects of both genders with the metabolic syndrome, with predominantly abdominal obesity, low-calorie regimens have not proved to be successful in long-term interventions (113). Physical activity of moderate intensity is not sufficient for effective weight control (114). Higher levels of exercise, particularly in combination with other lifestyle modifications, have been shown to reduce the risk of developing DM in individuals with glucose intolerance (115). The improvement in insulin sensitivity and muscle mass, as well as the reduction in VAT, is less likely to be explained by caloric restriction or increased exercise, as the participants did not receive any dietary intervention and did not show any change in physical activity. It can be summarized that assessment of body composition by CT is an

important tool for the understanding of the associations between morphological and hormonal factors in the metabolic syndrome and its treatment.

Measurements of body composition

Computed tomography for body composition and radiation dose reduction

In body composition studies with a single-slice CT technique, reliable area measures and CT numbers can be obtained with a radiation dose of only 2– 60 % of the radiation doses resulting from standard clinical scan parameters. The total radiation dose with the proposed patient specific scan parameters resulted in a calculated effective radiation dose for a single slice of <0.1 mSv, equating to the dose delivered by natural background radiation in a few weeks (116). At such a low risk level, CT for body composition can also be justified in research investigating larger populations. The proposed scheme also makes it possible to perform whole-body investigations as described in paper II (74, 75) with an effective radiation dose of less than 2 mSv. For lean to normally built persons, the effective radiation dose is considerably lower. It is also possible to justify CT examinations on wider indications for clinical patients and for performing repeated examinations over time as in paper III and IV. If radiation dose needs to be avoided altogether, the whole-body MR T_1 mapping method proposed in paper II, can be used.

Whole-body MRI for body composition

The proposed method for MRI, T_1 mapping body composition that allows a high degree of automated post-processing was validated with the results from a whole-body CT protocol as reference. The MRI method gave measurements of total AT volumes with only small differences from the whole-body CT method. The whole-body MRI T_1 mapping method, proposed in paper II, gave reliable results and can thus be used in assessment of body composition in research and clinical settings. Due to its absence of ionizing radiation, the method is suitable for use in longitudinal studies, even when children and adolescents are included.

Assessment of body composition on a tissue level

Whole body techniques, CT or MRI, for determination of tissues provide valuable information that is hard to obtain by surrogate measures. However, they are still foremost research tools. Single slice evaluation of adipose tissue shows a high correlation with VAT volume (49, 57, 117). In the limited material in paper II the correlation was r=0.967 which is comparable to these results, figure 15. In the placebo controlled trial of GH treatment of postmenopausal women with central adiposity, the changes and differences in VAT would not have been detected by other anthropometric measures that have been used as surrogates for VAT, *i.e.* BMI, waist circumference, sagittal diameter or waist-hip ratio. This study thus demonstrates the value of accurate assessment of body composition. A limit of 130 cm^2 has been suggested as a marker of an increased VAT level that constitutes an increased risk of cardiovascular morbidity (60, 118). Karelis and co-workers observed that VAT area by CT was larger in the group showing three or more features of the metabolic syndrome, table 2, than in those with a lower number of features (119). Furthermore, they showed that statistical control for two of the features, *i.e.* visceral fat and fasting triglycerides (but not total body fatness and/or waist circumference) abolished the differences in insulin sensitivity among obese postmenopausal women categorized for the severity of the metabolic syndrome.

Based on the findings in study IV, a potential improvement in clinical studies concerning obesity, the metabolic syndrome and T2D could be to use the CT derived VAT area as one of the inclusion criteria. With the proposed radiation dose reduction scheme, a single slice could be justified in examining obese patients. With an added scan ad mid liver level an assessment of hepatic fat content can be obtained and obese persons with an increased risk of developing chronic liver disease could possibly be detected early and preventive measures could be intensified. CT assessment might also have a potential to help to identify obese persons at increased risk of developing the metabolic syndrome or T2D. Single slice CT performed with reduced radiation dose thereby should be sufficient, since it is easy to perform and analyse and carries negligible risk for harmful effects caused by

ionizing radiation (116). The more elaborate whole body methods are still costly and time consuming even if there is promising development in reducing MRI scanning times (120-122). Combined with automated post-processing, this can develop into a method usable for larger patient groups (47, 96). So far the present technique has been proven useful in a study of lipid mobilization following Roux-en-Y gastric bypass (123).

Future perspectives

Further developments in imaging techniques will probably not focus so much on the basic adipose tissue quantifications. The new dual energy computed tomography technique might, however, improve contrast resolution of tissues and thereby make it possible to reduce the effective dose further. Body composition methods for tissue determinations have been research tools for a long time but possible clinical applications could be investigated. For instance, the usefulness of the single slice, low dose method, to assess and select obese patients for treatment alternatives could be evaluated. For research, methods are being developed to assess "new" compartments that are of interest for body composition researchers. Relationship with features of the metabolic syndrome and insulin resistance has been shown with fat between muscle bundles (15, 124, 125) and perivascular fat (126). Arrhythmogenic right ventricular dysplasia is associated with epicardial fat (127). Brown adipose tissue might be possible to assess using FDG PET-CT due to its increased metabolic activity (128). Fat in organs has also been assessed using ^{1}H magnetic resonance spectroscopy in the liver (129), myocardium (130), and muscle (131). For the question of fibrosis MR and ultrasound elastography could be developed into safe, non-invasive techniques with excellent diagnostic potential for assessing hepatic fibrosis (132, 133). A clinical application may be to assess patients who are under consideration for biopsy. A new quantitative magnetic resonance equipment used to determine whole-body fat and lean mass in humans is being evaluated (134).

Conclusions

I. In assessment of body composition using CT, the radiation dose to the subject can be reduced to 2-60 % of the standard radiation dose used for diagnostic purposes while maintaining accurate measurements of adipose tissue areas, muscle tissue areas, and muscle tissue attenuation. The resulting effective dose for a single slice examination is <0.1 mSv, a dose level associated with trivial risk. At such a low risk level, CT for assessment of body composition can be justified even in large populations or for repeated examinations.

II. Compared with CT, the MRI method slightly overestimated subcutaneous adipose tissue volume and slightly underestimated visceral adipose tissue volumes, but it can be considered sufficiently accurate for measurements of adipose tissue volumes in assessment of body composition.

III. The within-scanner reproducibility and between-scanner agreement were high for measurements of adipose and muscle tissue area by CT. For measurements of liver attenuation, the within-scanner reproducibility was high while a systematic bias was revealed in comparison between scanners. Therefore, comparisons of CT numbers for liver from different scanners can be unreliable.

IV. GH treatment of postmenopausal women with abdominal obesity reduced visceral adipose tissue and improved insulin sensitivity. CT revealed adipose tissue changes not detectable by waist-to-hip ratio, sagittal diameter, or waist circumference.

Acknowledgements

This thesis is not the project of one man but the result of inspiring teamwork. Every person of the team has contributed with his or her excellent knowledge, skills, and work. Many others collaborated with me in science through the years and that has been a great inspiration in the work with this thesis.

I wish to express my gratitude to my supervisor Lars Lönn for introducing me into the field of human body composition using imaging methods. He has always been supportive and generous. He has been introducing new ideas and projects throughout the years.

I also wish to express my gratitude to my assisting supervisors:
Lars Sjöström for providing working facilities, enthusiastic encouragement, fruitful discussions, and for generously sharing his vast knowledge.
Göran Starck for introducing me to physics of imaging and guiding me through difficulties with patience in the endeavour of science.
Malin Lönn for support, encouragement, and valuable criticism.

I wish to express my gratitude co-authors and co-workers:

Eva Forssell-Aronsson, co-author of paper I, for her support and valuable criticism. Eva Bergelin, co-author of paper I and II. Lena Strid, co-author of paper II, and Maria Cedhagen for performing the computed tomography procedures carefully analysing the images.

Joel Kullberg, co-author of paper II, for his never-ending enthusiasm, valuable discussions, and tireless energy. I also wish to thank the other co-authors and collaborators in Uppsala, Håkan Ahlström, Hans Frimmel, and Lars Johansson. I wish to thank the staff at the Magnetic Resonance Centre. Stig Eriksson for performing the MRI and Maria Ljungberg for assisting with the Physics.

Jan-Erik Angelhed, co-author of paper III, for fruitful discussions, support and air line services. He is also a master of computer programming, who actually can make a computer to do as you wish Helén Lantz, co-author of paper III, for collection of data and encouragement in the work with computed tomography and DXA. Matty Hellqvist skilfully performing DXA measurements.
Jarl Torgerson, co-author of paper III, for valuable criticism and generous support in all projects.

Celina Franco and Gudmundur Johannsson, co-authors of paper IV, for their invaluable guidance in endocrinology research and for interesting discussions of the importance of body composition changes. I also wish to thank the other co-authors, Björn Andersson and Bengt-Åke Bengtsson. The staff at Research Centre for Endocrinology and Metabolism are thanked for their excellent collaboration.

I wish to give a special thank to Mikael Hellström, head of department. I have been encouraged by his friendly support and care throughout the years but above all for his valuable scientific advice. He is a professor of integrity, a true friend, and has willingly put in the extra effort when it was needed. Lena Björneld for reading the proof of the manuscript for the thesis. Lotta Robertsson, who has been my guide in the University administration. For excellent library assistance Björn Gymnander, department of radiology and the staff at the clinical library Sahlgrenska University Hospital.

Research colleagues and staff at SOS secretariat and CMC:
Björn Fagerberg and Kaj Stenlöf for providing working facilities and support.
Heléne Berteus Forslund, Einar Björnsson, Björn Carlsson, Lena Carlsson, Ingalill Friis-Liby Anders Gummesson, Peter Jacobson, Kristjan Karason, Ingrid Larsson, Anna Karin Lindros, Ted Lystig, Markku Peltonen; Kristina Narbro, Pär Parén, and Tom William-Olsson for valuable discussions. Lisbeth Eriksson at the SOS secretariat, who knows everything, can find anything, and fix things

immediately. I also wish to thank the rest of the staff at the SOS secretariat and CMC, former “utvecklingslaboratoriet”, for support in every possible way.

I am grateful to all the staff members in the Radiology department. Special thanks to staff and colleagues at the Section of Abdominal and interventional radiology, who have encouraged and supported me Mats Andersson, Mats Asztély, Barbara Bergman, Paul Businge, Per Carlson, Mårten Falkenberg, Lilian Hammarstedt, Farida Hashimi, Olof Henrikson, Szérena Horváth, Ilja Laesser, Henrik Leonhardt, Augustinas Sakinis, Charlotte Sandström , Joanna Sternal, Fredrik Thorén, and Karin Zachrisson. Special thanks to Kjell Geterud, who despite the workload at the section allocated time for my research. Zlatica Radovanov, for encouragement.

I also which to thank Anne Olmarker, and the rest of “Röntgenledningen” who supported me and allowing me time to write.

Our friends and neighbours Birgitta and Jan. Without your support, it would not have been possible.

I also wish to thank my parents Åke and Gitten for support and immediate domestic assistance when needed. Gitten also provided me with her books about statistics and method comparison.

Above all I am very grateful for the love and support of my family. My wife has supported me and been kind to put in the extra effort needed at home when I have been doing my research. Love and a hug from a beautiful woman can do wonders for a tiered scientist. My children Carl, Erik, and Oskar are the true wonders of my world. Leia is always happy, even when I come home late at night.

Sammanfattning på svenska

Datortomografi (DT) och magnetisk resonanstomografi (MR) är bildgivande metoder som har ett brett användningsområde inom medicinen. Med hjälp av DT och MR kan till exempel kroppens olika vävnader framställas. Förändringar av dessa vävnaders storlek kan också följas över tid. För studier av kroppssammansättning, har teknikerna använts sedan 1980-talet.

Fetma utgör ett stort folkhälsoproblem. Förekomsten av fetma har ökat i världen och i Sverige. Idag lider ca 10 % av den svenska befolkningen av fetma. En ökad mängd fettvävnad inne i bukhålan, så kallat visceralt fett, är kopplad till det metabola syndromet, ett tillstånd som dessutom kännetecknas av nedsatt insulinkänslighet, högt blodtryck och förhöjda blodfetter. Tillståndet ökar risken för utveckling av typ 2 diabetes. Patienter med fetma och det metabola syndromet har också ofta en ökad mängd fett i levern som i sin tur kan leda till inflammation i levern och ”skrumplever”, ett tillstånd som kan kräva transplantation. Tillväxthormon som bildas i hypofysen har tydliga effekter på kropps-sammansättningen. Tillstånd med brist på tillväxthormon uppvisar många likheter med det metabola syndromet. För att öka kunskapen om fetma och dess följdsjukdomar, och kunna följa effekterna av nya behandlingsalternativ är det viktigt att ha tillgång till tillförlitlig och noggrann teknik för undersökning av kroppssammansättning.

En nackdel med datortomografi för bestämning av kroppssammansättning är att individen som undersöks utsätts för joniserande strålning. Generellt gäller att man ska använda en stråldos som är så låg som möjligt men ändå ger användbara resultat. Vid undersökning med DT utnyttjas att varje vävnad har ett karakteristiskt mätvärde som främst är beroende av vävnadens täthet. Detta värde kallas attenueringsvärde och används vid bestämning av kroppssammansättning för att skilja olika vävnadstyper åt, till exempel fett- och muskelvävnad. Motsvarande absoluta mätvärden erhålls ej vid MR-undersökningar där vävnaderna istället har en varierande och relativ signalintensitet. Då signalintensiteten varierar inom en och samma individ, så har MR haft en viktig begränsning jämfört med DT. En MR-metod har utvecklats som mäter den så kallade T_1 relaxationstiden vilket resulterar i mer specifika vävnadsmätningar.

Syftet med och resultaten från de underökningar som redovisas i denna avhandling var:

I. Att undersöka om det är möjligt att minska stråldosen vid undersökning av kroppssammansättning med DT genom att anpassa tekniken efter individens storlek. Tio patienter av olika storlek undersöktes vid standardiserad och reducerad stråldosnivå. Studien visade att stråldosen kan reduceras med 2-60 % av standardnivån utan att nämnvärt påverka mätvärdena för fett- och muskelvävnad.

II. Att jämföra en MR-metod, som bestämmer T_1 relaxationstiden, med en DT-metod vid helkroppsundersökningar av kroppssammansättning. Tio patienter undersöktes med bägge teknikerna. Resultaten visade att överensstämmelsen mellan teknikerna var god. Jämfört med DT förelåg en mindre överskattning av mängden underhudsfett och en mindre underskattning av visceralt fett.

III. Att undersöka om en datortomograf ger samma resultat vid upprepad mätning, och om två olika datortomografer ger samma resultat vid bestämning av kroppssammansättning. Femtio patienter undersöktes två gånger efter varandra med en datortomograf, därefter upprepades underökningarna med en annan datortomograf. Varje enskild utrustning visade god överensstämmelse mellan mätningarna. Det fanns också en god överensstämmelse mellan utrustningarna när mängden fettvävnad och muskelvävnad bestämdes. Det karakteristiska mätvärdet, attenueringsvärdet, för lever skiljde sig mellan utrustningarna.

IV. Att studera om tillväxthormonbehandling har gynnsamma effekter hos postmenopausala kvinnor med bukfetma. Fyrtio kvinnor fick under ett år med tillväxthormonbehandling eller placebo. Behandlingens effekter på kroppssammansättning, mätt med DT, och så kallad insulinkänslighet undersöktes. Resultaten visade att den viscerala fettmängden minskade medan muskelmängden ökade under behandlingen med tillväxthormon. Kvinnor som fick tillväxthormon fick också en ökad insulinkänslighet och man fann ett samband mellan förbättrad insulinkänslighet och minskad leverförfettning. Sammanfattningsvis visar studierna att det är viktigt att utveckla och förfina teknik för bestämning av kroppssammansättning. Användning av denna teknik ger inte bara information om kroppens sammansättning i sig, utan kan också bidra till värdefull kunskap om processer med betydelse för hälsa och sjukdomsutveckling.

Appendix

2. L 4, Trunk

CL 03 All tissues(AR68,40,04,08,13,28,CI65 and DI55,56)
The determination line is drawn in surrounding air and circumscribes all tissues. (Automatic)

AR	68	Total area of all tissues and gas		cm^2
AR	40	% visible skin circumference		%
CI	65	Circumference		mm
DI	55	Sagittal diameter		mm
DI	56	Transversal diameter		mm
AR	04	MT total skin, muscles, organs, spinal channel and RBM	-29 to +151 HU	cm^2
AR	08	AT total subcutaneous, intermuscular, intraabdominal and WBM	-190 to -30 HU	cm^2
AR	13	BT total bone tissue and calcification.	+152 to +2500 HU	cm^2
AR	28	Gas intraabdominal	-191 to -1000 HU	cm^2

AR 70 BT vertebra +152 to +2500 HU cm^2
The determination line circumscribes vertebra bone tissue. (Manual)

AR 01 Muscles, organs and RBM -29 to +151 HU cm^2
The determination line is drawn in the subcutaneous adipose tissue and circumscribes muscles and organs. (Automatic)

AR 45 AT intermuscular, intraabdominal and WBM -190 to -30 HU cm^2
The determination line is adjusted to the muscle fascia and circumscribes muscles and adipose tissue inside fascia. Do not include subcutaneous adipose tissue. (Manual)

AR 26 AT intraabdominal -190 to -30 HU cm^2
The determination line is drawn in the muscle bone wall of the trunk. Draw the line on the inside border of the rectus abdominal muscles, the transversal abdominal muscles, the iliac crests, the quadratus lumbar muscles, muscle of psoas and the anterior aspect of the vertebral body. Do not include adipose tissue between muscle bundles. (Manual)

AR 44 AT intraperitoneal -190 to -30 HU cm^2

The determination line is drawn in muscles and an invisible line in abdominal adipose tissue and circumscribes the intra peritoneal area. Ventrally use the determination line described in AR 26. Find the point between the rectus muscle and the transversal abdominal muscle and draw the line in the abdominal adipose tissue to the lateral aspects of colon. Encircle the colon and then proceed between the intestines and the muscle of psoas. The line is continued between intestines and the great vessels to the contralateral side where the line is drawn likewise. Do not include adipose tissue posterior to colon or the iliac vessels. (Manual)

AR 27 AT in triangular pad -190 to -30 HU cm^2

Use the determination line as described in AR 26 or AR44 as anterior border. Find the thickest parts of the rectus abdominal muscles and join them with a line. If the line crosses intestines, then move the line ventrally. (Manual)

AR 29 Organs abdominal -29 to +151 HU cm^2

The determination line is drawn in the adipose tissue inside the muscle bone wall of the trunk and circumscribes the visceral organs. Do not include muscles. (Manual)

CL 06 Bone marrow (AR16,19)

The determination line is drawn in cortical bone. (Automatic)

AR 16 White bone marrow (WBM) -190 to -30 HU cm^2

AR 19 Red bone marrow (RBM) -29 to +151 HU cm^2

AR 43 Spinal channel -29 to +151 HU cm^2

The determination line is drawn in cortical bone and circumscribes the spinal channel. Close scattered lines in the spinal channel border. (Manual)

References

1. Walstam R. Svensk radiologisk fysik - i min backspegel; 1996.
2. Richmond C. Sir Godfrey Hounsfield 10.1136/bmj.329.7467.687. BMJ 2004;329(7467):687-.
3. Greitz T. Intryck från ett halvt sekel svensk neuroradiologi; 1988.
4. Clinical guidelines on the identification, evaluation, and treatment of overweight and obesity in adults: executive summary. Expert Panel on the Identification, Evaluation, and Treatment of Overweight in Adults. Am J Clin Nutr 1998;68(4):899-917.
5. Raftopoulos I, Ercole J, Udekwu AO, Luketich JD, Courcoulas AP. Outcomes of Roux-en-Y gastric bypass stratified by a body mass index of 70 kg/m2: a comparative analysis of 825 procedures. J Gastrointest Surg 2005;9(1):44-52; discussion 52-3.
6. Obesity: preventing and managing the global epidemic. Geneva: World Health Organization; 2004.
7. Ogden CL, Carroll MD, Curtin LR, McDowell MA, Tabak CJ, Flegal KM. Prevalence of overweight and obesity in the United States, 1999-2004. Jama 2006;295(13):1549-55.
8. Neovius M, Janson A, Rossner S. Prevalence of obesity in Sweden. Obes Rev 2006;7(1):1-3.
9. Sjostrom LV. Mortality of severely obese subjects. Am J Clin Nutr 1992;55(2 Suppl):516S-523S.
10. Sjostrom LV. Morbidity of severely obese subjects. Am J Clin Nutr 1992;55(2 Suppl):508S-515S.
11. Sjostrom L, Narbro K, Sjostrom CD, Karason K, Larsson B, Wedel H, et al. Effects of bariatric surgery on mortality in Swedish obese subjects. N Engl J Med 2007;357(8):741-52.
12. Kumanyika S, Jeffery RW, Morabia A, Ritenbaugh C, Antipatis VJ. Obesity prevention: the case for action. Int J Obes Relat Metab Disord 2002;26(3):425-36.
13. Machann J, Thamer C, Schnoedt B, Stefan N, Stumvoll M, Haring HU, et al. Age and gender related effects on adipose tissue compartments of subjects with increased risk for type 2 diabetes: a whole body MRI/MRS study. Magma 2005;18(3):128-37.
14. Brochu M, Starling RD, Tchernof A, Matthews DE, Garcia-Rubi E, Poehlman ET. Visceral adipose tissue is an independent correlate of glucose disposal in older obese postmenopausal women. J Clin Endocrinol Metab 2000;85(7):2378-84.
15. Goodpaster BH, Thaete FL, Kelley DE. Thigh adipose tissue distribution is associated with insulin resistance in obesity and in type 2 diabetes mellitus. Am J Clin Nutr 2000;71(4):885-92.
16. Marchesini G, Brizi M, Bianchi G, Tomassetti S, Bugianesi E, Lenzi M, et al. Nonalcoholic fatty liver disease: a feature of the metabolic syndrome. Diabetes 2001;50(8):1844-50.
17. Goodpaster BH, Thaete FL, Kelley DE. Composition of skeletal muscle evaluated with computed tomography. Ann N Y Acad Sci 2000;904:18-24.
18. Reaven GM. Banting lecture 1988. Role of insulin resistance in human disease. Diabetes 1988;37(12):1595-607.
19. Alberti KG, Zimmet P, Shaw J. Metabolic syndrome--a new world-wide definition. A Consensus Statement from the International Diabetes Federation. Diabet Med 2006;23(5):469-80.
20. Alberti KG, Zimmet PZ. Definition, diagnosis and classification of diabetes mellitus and its complications. Part 1: diagnosis and classification of diabetes mellitus provisional report of a WHO consultation. Diabet Med 1998;15(7):539-53.
21. Executive Summary of The Third Report of The National Cholesterol Education Program (NCEP) Expert Panel on Detection, Evaluation, And Treatment of High Blood Cholesterol In Adults (Adult Treatment Panel III). Jama 2001;285(19):2486-97.

22. Grundy SM, Brewer HB, Jr., Cleeman JI, Smith SC, Jr., Lenfant C. Definition of metabolic syndrome: Report of the National Heart, Lung, and Blood Institute/American Heart Association conference on scientific issues related to definition. Circulation 2004;109(3):433-8.
23. Alberti KG, Zimmet P, Shaw J. The metabolic syndrome--a new worldwide definition. Lancet 2005;366(9491):1059-62.
24. Yu AS, Keeffe EB. Nonalcoholic fatty liver disease. Rev Gastroenterol Disord 2002;2(1):11-9.
25. Adams LA, Angulo P, Lindor KD. Nonalcoholic fatty liver disease. Cmaj 2005;172(7):899-905.
26. Wanless IR, Lentz JS. Fatty liver hepatitis (steatohepatitis) and obesity: an autopsy study with analysis of risk factors. Hepatology 1990;12(5):1106-10.
27. Ludwig J, Viggiano TR, McGill DB, Oh BJ. Nonalcoholic steatohepatitis: Mayo Clinic experiences with a hitherto unnamed disease. Mayo Clin Proc 1980;55(7):434-8.
28. Ekstedt M, Franzen LE, Mathiesen UL, Thorelius L, Holmqvist M, Bodemar G, et al. Long-term follow-up of patients with NAFLD and elevated liver enzymes. Hepatology 2006;44(4):865-73.
29. Schreuder TC, Verwer BJ, van Nieuwkerk CM, Mulder CJ. Nonalcoholic fatty liver disease: An overview of current insights in pathogenesis, diagnosis and treatment. World J Gastroenterol 2008;14(16):2474-86.
30. Vahl N, Jorgensen JO, Skjaerbaek C, Veldhuis JD, Orskov H, Christiansen JS. Abdominal adiposity rather than age and sex predicts mass and regularity of GH secretion in healthy adults. Am J Physiol 1997;272(6 Pt 1):E1108-16.
31. Salomon F, Cuneo RC, Hesp R, Sonksen PH. The effects of treatment with recombinant human growth hormone on body composition and metabolism in adults with growth hormone deficiency. N Engl J Med 1989;321(26):1797-803.
32. Johansson JO, Fowelin J, Landin K, Lager I, Bengtsson BA. Growth hormone-deficient adults are insulin-resistant. Metabolism 1995;44(9):1126-9.
33. Johannsson G, Marin P, Lonn L, Ottosson M, Stenlof K, Bjorntorp P, et al. Growth hormone treatment of abdominally obese men reduces abdominal fat mass, improves glucose and lipoprotein metabolism, and reduces diastolic blood pressure. J Clin Endocrinol Metab 1997;82(3):727-34.
34. Albert SG, Mooradian AD. Low-dose recombinant human growth hormone as adjuvant therapy to lifestyle modifications in the management of obesity. J Clin Endocrinol Metab 2004;89(2):695-701.
35. Lonn L, Johansson G, Sjostrom L, Kvist H, Oden A, Bengtsson BA. Body composition and tissue distributions in growth hormone deficient adults before and after growth hormone treatment. Obes Res 1996;4(1):45-54.
36. Brummer RJ, Lonn L, Kvist H, Grangard U, Bengtsson BA, Sjostrom L. Adipose tissue and muscle volume determination by computed tomography in acromegaly, before and 1 year after adenomectomy. Eur J Clin Invest 1993;23(4):199-205.
37. Wang ZM, Pierson RN, Jr., Heymsfield SB. The five-level model: a new approach to organizing body-composition research. Am J Clin Nutr 1992;56(1):19-28.
38. Smalley KJ, Knerr AN, Kendrick ZV, Colliver JA, Owen OE. Reassessment of body mass indices. Am J Clin Nutr 1990;52(3):405-8.
39. Prentice AM, Jebb SA. Beyond body mass index. Obes Rev 2001;2(3):141-7.
40. Stanforth PR, Jackson AS, Green JS, Gagnon J, Rankinen T, Despres JP, et al. Generalized abdominal visceral fat prediction models for black and white adults aged 17-65 y: the HERITAGE Family Study. Int J Obes Relat Metab Disord 2004;28(7):925-32.
41. Wang J, Thornton JC, Kolesnik S, Pierson RN, Jr. Anthropometry in body composition. An overview. Ann N Y Acad Sci 2000;904:317-26.
42. Bosaeus I, Johannsson G, Rosen T, Hallgren P, Tolli J, Sjostrom L, et al. Comparison of methods to estimate body fat in growth hormone deficient adults. Clin Endocrinol (Oxf) 1996;44(4):395-402.

43. Sjostrom L, Kvist H, Cederblad A, Tylen U. Determination of total adipose tissue and body fat in women by computed tomography, 40K, and tritium. Am J Physiol 1986;250(6 Pt 1):E736-45.
44. Watson WS. Total body potassium measurement--the effect of fallout from Chernobyl. Clin Phys Physiol Meas 1987;8(4):337-41.
45. Kalender WA. Computed Tomography Fundamentals, System Technology, Image quality, Applications. 2nd ed. Erlangen: Publicis Corporate Publishing; 2005.
46. McRobbie DW, Moore EA, Graves M, Prince M. MRI From Picture to Proton. Second 2007 ed. Cambridge: Cambridge University Press; 2003.
47. Kullberg J, Angelhed JE, Lonn L, Brandberg J, Ahlstrom H, Frimmel H, et al. Whole-body T1 mapping improves the definition of adipose tissue: consequences for automated image analysis. J Magn Reson Imaging 2006;24(2):394-401.
48. Chowdhury B, Kvist H, Andersson B, Bjorntorp P, Sjostrom L. CT-determined changes in adipose tissue distribution during a small weight reduction in obese males. Int J Obes Relat Metab Disord 1993;17(12):685-91.
49. Kvist H, Chowdhury B, Grangard U, Tylen U, Sjostrom L. Total and visceral adipose-tissue volumes derived from measurements with computed tomography in adult men and women: predictive equations. Am J Clin Nutr 1988;48(6):1351-61.
50. Kvist H, Chowdhury B, Sjostrom L, Tylen U, Cederblad A. Adipose tissue volume determination in males by computed tomography and 40K. Int J Obes 1988;12(3):249-66.
51. Tokunaga K, Matsuzawa Y, Ishikawa K, Tarui S. A novel technique for the determination of body fat by computed tomography. Int J Obes 1983;7(5):437-45.
52. Borkan GA, Hults DE, Gerzof SG, Burrows BA, Robbins AH. Relationships between computed tomography tissue areas, thicknesses and total body composition. Ann Hum Biol 1983;10(6):537-45.
53. Mitsiopoulos N, Baumgartner RN, Heymsfield SB, Lyons W, Gallagher D, Ross R. Cadaver validation of skeletal muscle measurement by magnetic resonance imaging and computerized tomography. J Appl Physiol 1998;85(1):115-22.
54. Chowdhury B, Sjostrom L, Alpsten M, Kostanty J, Kvist H, Lofgren R. A multicompartment body composition technique based on computerized tomography. Int J Obes Relat Metab Disord 1994;18(4):219-34.
55. Lonn L, Starck G, Alpsten M, Ekholm S, Sjostrom L. Determination of tissue volumes. A comparison between CT and MR imaging. Acta Radiol 1999;40(3):314-21.
56. Shen W, Wang Z, Punyanita M, Lei J, Sinav A, Kral JG, et al. Adipose tissue quantification by imaging methods: a proposed classification. Obes Res 2003;11(1):5-16.
57. Kuk JL, Church TS, Blair SN, Ross R. Does measurement site for visceral and abdominal subcutaneous adipose tissue alter associations with the metabolic syndrome? Diabetes Care 2006;29(3):679-84.
58. Foster MA, Hutchison JM, Mallard JR, Fuller M. Nuclear magnetic resonance pulse sequence and discrimination of high- and low-fat tissues. Magn Reson Imaging 1984;2(3):187-92.
59. Hayes PA, Sowood PJ, Belyavin A, Cohen JB, Smith FW. Sub-cutaneous fat thickness measured by magnetic resonance imaging, ultrasound, and calipers. Med Sci Sports Exerc 1988;20(3):303-9.
60. Ross R, Leger L, Morris D, de Guise J, Guardo R. Quantification of adipose tissue by MRI: relationship with anthropometric variables. J Appl Physiol 1992;72(2):787-95.
61. Thomas EL, Saeed N, Hajnal JV, Brynes A, Goldstone AP, Frost G, et al. Magnetic resonance imaging of total body fat. J Appl Physiol 1998;85(5):1778-85.
62. Bydder GM, Kreel L, Chapman RW, Harry D, Sherlock S, Bassan L. Accuracy of computed tomography in diagnosis of fatty liver. Br Med J 1980;281(6247):1042.
63. Ricci C, Longo R, Gioulis E, Bosco M, Pollesello P, Masutti F, et al. Noninvasive in vivo quantitative assessment of fat content in human liver. J Hepatol 1997;27(1):108-13.

64. Ducommun JC, Goldberg HI, Korobkin M, Moss AA, Kressel HY. The relation of liver fat to computed tomography numbers: a preliminary experimental study in rabbits. Radiology 1979;130(2):511-3.
65. Goodpaster BH, Thaete FL, Simoneau JA, Kelley DE. Subcutaneous abdominal fat and thigh muscle composition predict insulin sensitivity independently of visceral fat. Diabetes 1997;46(10):1579-85.
66. Goodpaster BH, Carlson CL, Visser M, Kelley DE, Scherzinger A, Harris TB, et al. Attenuation of skeletal muscle and strength in the elderly: The Health ABC Study. J Appl Physiol 2001;90(6):2157-65.
67. Hughes JS, Watson SJ, Jones AL, Oatway WB. Review of the radiation exposure of the UK population. J Radiol Prot 2005;25(4):493-6.
68. Huda W, Scalzetti EM, Levin G. Technique factors and image quality as functions of patient weight at abdominal CT. Radiology 2000;217(2):430-5.
69. Buntinx F, Knottnerus JA. Are we at the start of a new era in diagnostic research? Journal of Clinical Epidemiology 2006;59(4):325-326.
70. Gagnon J, Province MA, Bouchard C, Leon AS, Skinner JS, Wilmore JH, et al. The HERITAGE Family Study: quality assurance and quality control. Ann Epidemiol 1996;6(6):520-9.
71. Yoshizumi T, Nakamura T, Yamane M, Islam AH, Menju M, Yamasaki K, et al. Abdominal fat: standardized technique for measurement at CT. Radiology 1999;211(1):283-6.
72. Hudash G, Albright JP, McAuley E, Martin RK, Fulton M. Cross-sectional thigh components: computerized tomographic assessment. Med Sci Sports Exerc 1985;17(4):417-21.
73. Torgerson JS, Hauptman J, Boldrin MN, Sjostrom L. XENical in the prevention of diabetes in obese subjects (XENDOS) study: a randomized study of orlistat as an adjunct to lifestyle changes for the prevention of type 2 diabetes in obese patients. Diabetes Care 2004;27(1):155-61.
74. Sjostrom L, Larsson B, Backman L, Bengtsson C, Bouchard C, Dahlgren S, et al. Swedish obese subjects (SOS). Recruitment for an intervention study and a selected description of the obese state. Int J Obes Relat Metab Disord 1992;16(6):465-79.
75. Larsson I, Berteus Forslund H, Lindroos AK, Lissner L, Naslund I, Peltonen M, et al. Body composition in the SOS (Swedish Obese Subjects) reference study. Int J Obes Relat Metab Disord 2004;28(10):1317-24.
76. Torgerson JS, Arlinger K, Kappi M, Sjostrom L. Principles for enhanced recruitment of subjects in a large clinical trial. the XENDOS (XENical in the prevention of Diabetes in Obese Subjects) study experience. Control Clin Trials 2001;22(5):515-25.
77. Starck G, Lonn L, Cederblad A, Forssell-Aronsson E, Sjostrom L, Alpsten M. A method to obtain the same levels of CT image noise for patients of various sizes, to minimize radiation dose. Br J Radiol 2002;75(890):140-50.
78. Starck G, Lonn L, Cederblad A, Alpsten M, Sjostrom L, Ekholm S. Radiation dose reduction in CT: application to tissue area and volume determination. Radiology 1998;209(2):397-403.
79. Starck G, Lonn L, Cederblad A, Alpsten M, Sjostrom L, Ekholm S. Dose reduction for body composition measurements with CT. Appl Radiat Isot 1998;49(5-6):561-3.
80. Kvist H, Sjostrom L, Tylen U. Adipose tissue volume determinations in women by computed tomography: technical considerations. Int J Obes 1986;10(1):53-67.
81. Lantz H, Samuelson G, Bratteby LE, Mallmin H, Sjostrom L. Differences in whole body measurements by DXA-scanning using two Lunar DPX-L machines. Int J Obes Relat Metab Disord 1999;23(7):764-70.
82. DeFronzo RA, Tobin JD, Andres R. Glucose clamp technique: a method for quantifying insulin secretion and resistance. Am J Physiol 1979;237(3):E214-23.
83. American Diabetes Association: clinical practice recommendations 1997. Diabetes Care 1997;20 Suppl 1:S1-70.

84. Haffner SM, Kennedy E, Gonzalez C, Stern MP, Miettinen H. A prospective analysis of the HOMA model. The Mexico City Diabetes Study. Diabetes Care 1996;19(10):1138-41.
85. Landin-Wilhelmsen K, Wilhelmsen L, Lappas G, Rosen T, Lindstedt G, Lundberg PA, et al. Serum insulin-like growth factor I in a random population sample of men and women: relation to age, sex, smoking habits, coffee consumption and physical activity, blood pressure and concentrations of plasma lipids, fibrinogen, parathyroid hormone and osteocalcin. Clin Endocrinol (Oxf) 1994;41(3):351-7.
86. Friedewald WT, Levy RI, Fredrickson DS. Estimation of the concentration of low-density lipoprotein cholesterol in plasma, without use of the preparative ultracentrifuge. Clin Chem 1972;18(6):499-502.
87. Bland JM, Altman DG. Statistical methods for assessing agreement between two methods of clinical measurement. Lancet 1986;1(8476):307-10.
88. Boone JM, Geraghty EM, Seibert JA, Wootton-Gorges SL. Dose reduction in pediatric CT: a rational approach. Radiology 2003;228(2):352-60.
89. Kalender WA, Wolf H, Suess C. Dose reduction in CT by anatomically adapted tube current modulation. II. Phantom measurements. Med Phys 1999;26(11):2248-53.
90. Kalender WA, Wolf H, Suess C, Gies M, Greess H, Bautz WA. Dose reduction in CT by on-line tube current control: principles and validation on phantoms and cadavers. Eur Radiol 1999;9(2):323-28.
91. Menke J. Comparison of different body size parameters for individual dose adaptation in body CT of adults. Radiology 2005;236(2):565-71.
92. Jones R, Payne B. Clinical investigation and statistics in laboratory medicin. London: ACB Venture publictions; 1997.
93. Altman D. Practical statistics for medical research. Boca Raton: Chapman & Hall; 1991.
94. Stockl D, Dewitte K, Thienpont LM. Validity of linear regression in method comparison studies: is it limited by the statistical model or the quality of the analytical input data? Clin Chem 1998;44(11):2340-6.
95. Potretzke AM, Schmitz KH, Jensen MD. Preventing overestimation of pixels in computed tomography assessment of visceral fat. Obes Res 2004;12(10):1698-701.
96. Kullberg J, Ahlstrom H, Johansson L, Frimmel H. Automated and reproducible segmentation of visceral and subcutaneous adipose tissue from abdominal MRI. Int J Obes (Lond) 2007;31(12):1806-17.
97. Stadler A, Schima W, Prager G, Homolka P, Heinz G, Saini S, et al. CT density measurements for characterization of adrenal tumors ex vivo: variability among three CT scanners. AJR Am J Roentgenol 2004;182(3):671-5.
98. Hahn PF, Blake MA, Boland GW. Adrenal lesions: attenuation measurement differences between CT scanners. Radiology 2006;240(2):458-63.
99. Svendsen OL. Body composition and fat distribution by dual energy X-ray absorptiometry in overweight postmenopausal women. Effect of energy-restriction and exercise. Dan Med Bull 1996;43(3):249-62.
100. Laskey MA. Dual-energy X-ray absorptiometry and body composition. Nutrition 1996;12(1):45-51.
101. Svendsen OL, Haarbo J, Hassager C, Christiansen C. Accuracy of measurements of body composition by dual-energy x-ray absorptiometry in vivo. Am J Clin Nutr 1993;57(5):605-8.
102. Genton L, Hans D, Kyle UG, Pichard C. Dual-energy X-ray absorptiometry and body composition: differences between devices and comparison with reference methods. Nutrition 2002;18(1):66-70.
103. Johannsson G, Albertsson-Wikland K, Bengtsson BA. Discontinuation of growth hormone (GH) treatment: metabolic effects in GH-deficient and GH-sufficient adolescent patients compared with control subjects. Swedish Study Group for Growth Hormone Treatment in Children. J Clin Endocrinol Metab 1999;84(12):4516-24.

104. Johannsson G, Bengtsson BA. Influence of gender and gonadal steroids on responsiveness to growth hormone replacement therapy in adults with growth hormone deficiency. Growth Horm IGF Res 1998;8 Suppl B:69-75.
105. Ferrara CM, Lynch NA, Nicklas BJ, Ryan AS, Berman DM. Differences in adipose tissue metabolism between postmenopausal and perimenopausal women. J Clin Endocrinol Metab 2002;87(9):4166-70.
106. Bjorntorp P. Endocrine abnormalities of obesity. Metabolism 1995;44(9 Suppl 3):21-3.
107. Bengtsson BA, Eden S, Lonn L, Kvist H, Stokland A, Lindstedt G, et al. Treatment of adults with growth hormone (GH) deficiency with recombinant human GH. J Clin Endocrinol Metab 1993;76(2):309-17.
108. Leander P, Sjoberg S, Hoglund P. CT and MR imaging of the liver. Clinical importance of nutritional status. Acta Radiol 2000;41(2):151-5.
109. Goto T, Onuma T, Takebe K, Kral JG. The influence of fatty liver on insulin clearance and insulin resistance in non-diabetic Japanese subjects. Int J Obes Relat Metab Disord 1995;19(12):841-5.
110. Hollis S. Analysis of method comparison studies. Ann Clin Biochem 1996;33 (Pt 1):1-4.
111. Elam MB, Wilcox HG, Solomon SS, Heimberg M. In vivo growth hormone treatment stimulates secretion of very low density lipoprotein by the isolated perfused rat liver. Endocrinology 1992;131(6):2717-22.
112. Rudling M, Parini P, Angelin B. Growth hormone and bile acid synthesis. Key role for the activity of hepatic microsomal cholesterol 7alpha-hydroxylase in the rat. J Clin Invest 1997;99(9):2239-45.
113. Marin P, Arver S. Androgens and abdominal obesity. Baillieres Clin Endocrinol Metab 1998;12(3):441-51.
114. Jakicic JM. Exercise in the treatment of obesity. Endocrinol Metab Clin North Am 2003;32(4):967-80.
115. Tuomilehto J, Lindstrom J, Eriksson JG, Valle TT, Hamalainen H, Ilanne-Parikka P, et al. Prevention of type 2 diabetes mellitus by changes in lifestyle among subjects with impaired glucose tolerance. N Engl J Med 2001;344(18):1343-50.
116. The International Commission on Radiological Protection (ICRP): Radiological Protection in Biomedical Research. ICRP publication 62. Oxford, UK: Pergamon Press; 1993.
117. Shen W, Punyanitya M, Chen J, Gallagher D, Albu J, Pi-Sunyer X, et al. Visceral adipose tissue: relationships between single slice areas at different locations and obesity-related health risks. Int J Obes (Lond) 2007;31(5):763-9.
118. Despres JP, Lamarche B. Low-intensity endurance exercise training, plasma lipoproteins and the risk of coronary heart disease. J Intern Med 1994;236(1):7-22.
119. Karelis AD, Henry JF, St-Pierre DH, Prud'homme D, Rabasa-Lhoret R. Degradation in insulin sensitivity with increasing severity of the metabolic syndrome in obese postmenopausal women. Diabetes Obes Metab 2006;8(3):336-41.
120. Kruger DG, Riederer SJ, Grimm RC, Rossman PJ. Continuously moving table data acquisition method for long FOV contrast-enhanced MRA and whole-body MRI. Magn Reson Med 2002;47(2):224-31.
121. Engelhard K, Hollenbach HP, Wohlfart K, von Imhoff E, Fellner FA. Comparison of whole-body MRI with automatic moving table technique and bone scintigraphy for screening for bone metastases in patients with breast cancer. Eur Radiol 2004;14(1):99-105.
122. Bornert P, Aldefeld B. Principles of whole-body continuously-moving-table MRI. J Magn Reson Imaging 2008;28(1):1-12.
123. Johansson L, Roos M, Kullberg J, Weis J, Ahlstrom H, Sundbom M, et al. Lipid mobilization following Roux-en-Y gastric bypass examined by magnetic resonance imaging and spectroscopy. Obes Surg 2008;18(10):1297-304.

124. Yim JE, Heshka S, Albu J, Heymsfield S, Kuznia P, Harris T, et al. Intermuscular adipose tissue rivals visceral adipose tissue in independent associations with cardiovascular risk. Int J Obes (Lond) 2007;31(9):1400-5.
125. Gallagher D, Kuznia P, Heshka S, Albu J, Heymsfield SB, Goodpaster B, et al. Adipose tissue in muscle: a novel depot similar in size to visceral adipose tissue. Am J Clin Nutr 2005;81(4):903-10.
126. Rittig K, Staib K, Machann J, Bottcher M, Peter A, Schick F, et al. Perivascular fatty tissue at the brachial artery is linked to insulin resistance but not to local endothelial dysfunction. Diabetologia 2008;51(11):2093-9.
127. Fattori R, Tricoci P, Russo V, Lovato L, Bacchi-Reggiani L, Gavelli G, et al. Quantification of fatty tissue mass by magnetic resonance imaging in arrhythmogenic right ventricular dysplasia. J Cardiovasc Electrophysiol 2005;16(3):256-61.
128. Hadi M, Chen CC, Whatley M, Pacak K, Carrasquillo JA. Brown fat imaging with (18)F-6-fluorodopamine PET/CT, (18)F-FDG PET/CT, and (123)I-MIBG SPECT: a study of patients being evaluated for pheochromocytoma. J Nucl Med 2007;48(7):1077-83.
129. Mehta SR, Thomas EL, Bell JD, Johnston DG, Taylor-Robinson SD. Non-invasive means of measuring hepatic fat content. World J Gastroenterol 2008;14(22):3476-83.
130. Kankaanpaa M, Lehto HR, Parkka JP, Komu M, Viljanen A, Ferrannini E, et al. Myocardial triglyceride content and epicardial fat mass in human obesity: relationship to left ventricular function and serum free fatty acid levels. J Clin Endocrinol Metab 2006;91(11):4689-95.
131. White LJ, Ferguson MA, McCoy SC, Kim H. Intramyocellular lipid changes in men and women during aerobic exercise: a (1)H-magnetic resonance spectroscopy study. J Clin Endocrinol Metab 2003;88(12):5638-43.
132. Gheorghe L, Iacob S, Gheorghe C. Real-time sonoelastography - a new application in the field of liver disease. J Gastrointestin Liver Dis 2008;17(4):469-74.
133. Yin M, Talwalkar JA, Glaser KJ, Manduca A, Grimm RC, Rossman PJ, et al. Assessment of hepatic fibrosis with magnetic resonance elastography. Clin Gastroenterol Hepatol 2007;5(10):1207-1213 e2.
134. Napolitano A, Miller SR, Murgatroyd PR, Coward WA, Wright A, Finer N, et al. Validation of a quantitative magnetic resonance method for measuring human body composition. Obesity (Silver Spring) 2008;16(1):191-8.